# Integrated Wideband Self-Interference Cancellation in the RF Domain for FDD and Full-Duplex Wireless

Jin Zhou, *Student Member, IEEE*, Tsung-Hao Chuang, *Student Member, IEEE*, Tolga Dinc, *Student Member, IEEE*, and Harish Krishnaswamy, *Member, IEEE*

*Abstract*—A fully integrated technique for wideband cancellation of transmitter (TX) self-interference (SI) in the RF domain is proposed for multiband frequency-division duplexing (FDD) and full-duplex (FD) wireless applications. Integrated wideband SI cancellation (SIC) in the RF domain is accomplished through: 1) a bank of tunable, reconfigurable second-order high-Q RF bandpass filters in the canceller that emulate the antenna interface's isolation (essentially frequency-domain equalization in the RF domain) and 2) a linear $N$-path $G_m$-$C$ filter implementation with embedded variable attenuation and phase shifting. A 0.8–1.4 GHz receiver (RX) with the proposed wideband SIC circuits is implemented in a 65 nm CMOS process. In measurement, >20 MHz 20 dB cancellation bandwidth (BW) is achieved across frequency-selective antenna interfaces: 1) a custom-designed LTE-like 0.780/0.895 GHz duplexer with TX/RX isolation peak magnitude of 30 dB, peak group delay of 11 ns, and 7 dB magnitude variation across the TX band for FDD and 2) a 1.4 GHz antenna pair for FD wireless with TX/RX isolation peak magnitude of 32 dB, peak group delay of 9 ns, and 3 dB magnitude variation over 1.36–1.38 GHz. For FDD, SIC enhances the effective out-of-band (OOB) IIP3 and IIP2 to +25–27 dBm and +90 dBm, respectively (enhancements of 8–10 and 29 dB, respectively). For FD, SIC eliminates RX gain compression for as high as −8 dBm of peak in-band (IB) SI, and enhances effective IB IIP3 and IIP2 by 22 and 58 dB.

*Index Terms*—Blocker, CMOS, coexistence, cross-modulation, frequency-division duplexing (FDD), frequency-domain equalization (FDE), full-duplex (FD), receiver (RX), SAW-less, self-interference (SI), SI cancellation (SIC), transmitter (TX) leakage, triple beat, wideband.

## I. INTRODUCTION

**M**ODERN wireless communication standards support numerous frequency bands. Consequently, wireless devices (e.g., smartphones) need to support frequency-division duplexing (FDD) operation across transmit–receive band pairs that range from several hundreds of megahertz to several gigahertz [1]. Multiband FDD operation requires numerous off-chip duplexers which limit the system form factor. Research efforts have been making progress toward tunable duplexers [2]. However, the incorporation of tunability is typically associated with an increase in loss. Consequently, tunable duplexers tend to have less transmitter/receiver (TX/RX) isolation for the same insertion loss when compared with fixed-frequency duplexers. To relax TX/RX isolation, self-interference (SI) cancellation (SIC) is required as depicted in Fig. 1(a) [2]–[5].

Full-duplex (FD) wireless has been drawing significant research attention [6]–[15]. FD operation involves simultaneous transmission and reception at the same frequency [Fig. 1(b)], potentially resulting in significant improvement in wireless network performance [6], [15]. However, the biggest challenge associated with FD wireless is the tremendous amount of SI on top of the desired signal. The SI has to be suppressed below the RX noise floor through isolation and cancellation as filtering the SI is not an option. Given +15 dBm TX output power, 20 MHz RX signal bandwidth (BW) and 5 dB RX noise figure, >111 dB SI suppression is required. While discrete-component-based demonstrations have established the feasibility of FD wireless [6], [7], only recently have there been demonstrations of fully integrated RFICs incorporating SIC for FD [9]–[11], [13]. A fully integrated CMOS implementation imposes constraints that render SIC techniques proposed in prior discrete-component-based implementations (e.g., [7]) not viable.

SIC can be performed in the antenna [13], [14], RF [2]–[5], [7], [10], [11], [13], analog/mixed-signal [12], and/or digital domains [7]. The benefit of SIC in the RF domain (Fig. 1), where a replica signal is tapped from the TX output and injected prior to RX downconversion, is that the cancellation signal includes all the nonidealities coming from the TX chain. Furthermore, the earlier the SIC, the more relaxed is the RX front-end linearity requirement.

One of the fundamental challenges associated with SIC at RF is the cancellation BW [3], [16] due to the frequency selectivity of the antenna interface. A conventional RF canceller with a programmable but frequency-flat magnitude and phase response [see Fig. 2(a)] can only emulate the antenna interface isolation at a single frequency point [3]–[5], [11]. Wideband SIC at RF based on time-domain equalization [see Fig. 2(b)] has been reported in [7] using discrete components. Multiple on-PCB transmission-line delays and variable attenuators have been used, essentially implementing an RF FIR filter [7]. However, generation of significant (nanosecond-scale) true time delay on silicon is fundamentally challenging due to the length of the transmission lines required and the lossy nature of the silicon substrate [17]. Equalization of a frequency-selective SI channel can be performed in the digital domain as well, and a dedicated cancellation path can up-convert the TX replica
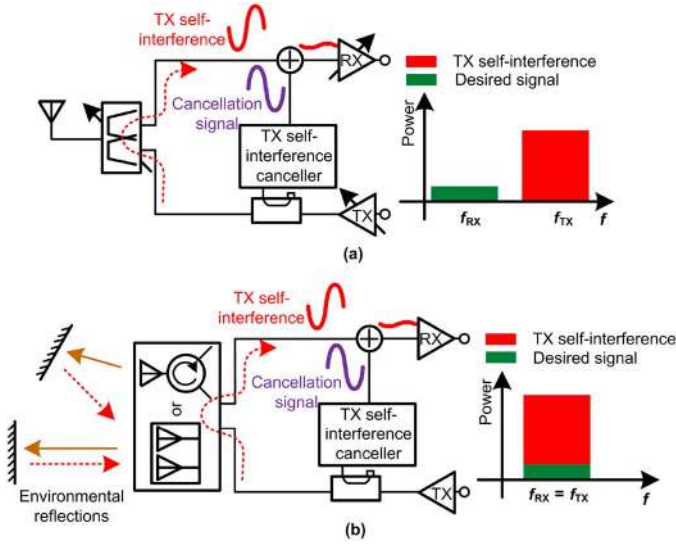
Fig. 1. TX SIC in the RF domain for (a) multiband FDD wireless system with a tunable duplexer and (b) FD wireless system.

signal to RF to perform SIC [12]. However, to suppress the TX distortion signals, this approach requires a recreation of the nonlinearity characteristics of the entire TX chain. Moreover, this approach is not able to cancel the noise from the TX chain.

We propose wideband SIC in the RF domain based on *frequency-domain equalization* (FDE) of the wireless SI channel as depicted in Fig. 2(d). Multiple RF bandpass filters (BPFs) are included in the canceller that channelize the desired signal BW. Within each channel, the BPF mimics the magnitude, phase, the slope of the magnitude, and the slope of the phase (i.e., group delay) of the wireless SI channel. The applicability of this technique to integrated wideband SIC in the RF domain is enabled by recent advances in the implementation of tunable, reconfigurable, high-$Q$ RF BPFs in nanoscale CMOS, namely $N$-path filters [18]–[20].

In [10], we reported a 0.8–1.4 GHz 65 nm CMOS RX that employed the proposed FDE-based canceller. The tunable, reconfigurable, second-order, high-$Q$ RF BPFs were realized as $N$-path $G_m$-$C$ filters [21] with embedded variable attenuation and phase shifting. Nearly $10\times$ improvement in cancellation BW is achieved over conventional frequency-flat amplitude- and phase-based RF cancellers across a pair of frequency-selective antenna interfaces: 1) a custom-designed LTE-like 0.780/0.895 GHz LC-based duplexer for FDD with 30 dB peak TX/RX isolation, 11 ns peak isolation group delay, and 7 dB isolation magnitude variation across the TX band and 2) a 1.4 GHz antenna pair for FD with 32 dB peak TX/RX isolation, 9 ns peak isolation group delay, and 3 dB isolation magnitude variation over 1.36 GHz to 1.38 GHz.

This paper is organized as follows. Section II discusses the system level considerations for FD wireless systems, with a focus on SIC in the RF domain. Section III describes the proposed FDE-based wideband SIC technique in the RF domain. Sections IV discusses the implementation of the 65 nm CMOS 0.8–1.4 GHz RX with the FDE-based SI canceller. Measurement results are given in Section V. Section VI concludes this paper.

## II. System-Level Analyses

An in-depth analysis of the system-level design tradeoffs and requirements for an FDD system with RF SIC have been discussed in [16]. The focus here is on an FD wireless system.

### A. FD System Considerations

In an integrated FD wireless transceiver as depicted in Fig. 3, the TX signal at the power amplifier (PA) output includes the TX main signal ($P_{\mathrm{TX,main}}$), TX nonlinear distortion signal ($P_{\mathrm{TX,dis}}$), and TX noise ($P_{\mathrm{TX,noise}}$). The TX signal leaks to the RX input (becoming SI) through an antenna interface with certain TX/RX isolation (ISO).

Assume that an FD wireless system with $P_{\mathrm{TX,main}} = +15$ dBm, 20 MHz RX BW, and 5 dB RX NF (NF$_{\mathrm{RX}}$), SIC of 15 dBm-(-174 dBm/Hz+5 dB+73 dBHz)+6 dB= 117 dB is required. Additional 6 dB cancellation has been assumed to ensure that the residual SI is well below the RX noise floor. Such a large amount of isolation/cancellation must be achieved by combining suppression at the antenna, and in RF, analog and digital domains. Although this work focuses on SIC in the RF domain, isolation and cancellation in all four domains are depicted in Fig. 3 to aid in system-level analysis.

SIC in the RF domain that taps from the PA output and cancels the SI at the RX front-end will cancel TX nonlinear distortion as well. However, the RF canceller might introduce its own nonlinear distortion ($P_{\mathrm{Canc,dis}}$ in Fig. 3). Depending on how much cancellation is achieved, the RX will introduce nonlinear distortion on the TX signal as well ($P_{\mathrm{RX,dis}}$ in Fig. 3). All these nonlinear distortions are predictable and can eventually be canceled in the digital domain [7]. What cannot be canceled in the digital domain are unpredictable effects of the SI, including RX gain compression of the desired signal, NF increase, and interaction between the SI (or nonlinear distortion generated in the RX and the canceller) and an unknown incoming continuous-wave (CW) jammer ($P_{\mathrm{jam}}$ in Fig. 3).[1] We assume that RF SIC suppresses the SI sufficiently to prevent gain compression of the desired signal (verified for our prototype in the measurement section) and NF increase. Hence, we focus on cross-modulation between the SI and an unknown jammer.

The analog cancellation is depicted as tapping from the PA output (similar to [11]). Therefore, it will further suppress not only the TX main signal but also the TX distortion and the TX noise. We assume that RF and analog SIC are sufficient to suppress the TX noise below the RX noise floor (see Fig. 3). RF canceller noise ($P_{\mathrm{Canc,noise}}$ in Fig. 3) needs to be considered as well in establishing the final RX noise floor in the FD system.

Fig. 4 illustrates the aforementioned 117 dB FD link budget enabled by SI isolation/cancellation across the various domains. The CW jammer and its associated cross-modulation distortion are not shown in Fig. 4 as they cannot be canceled. We assume that the RX and RF cancellers are designed so that their distortions ($P_{\mathrm{RX,dis}}$ and $P_{\mathrm{Canc,dis}}$) have the same power level as the residual SI after RF and

---

[1]This *cross-modulation distortion* is commonly considered in existing FDD systems.
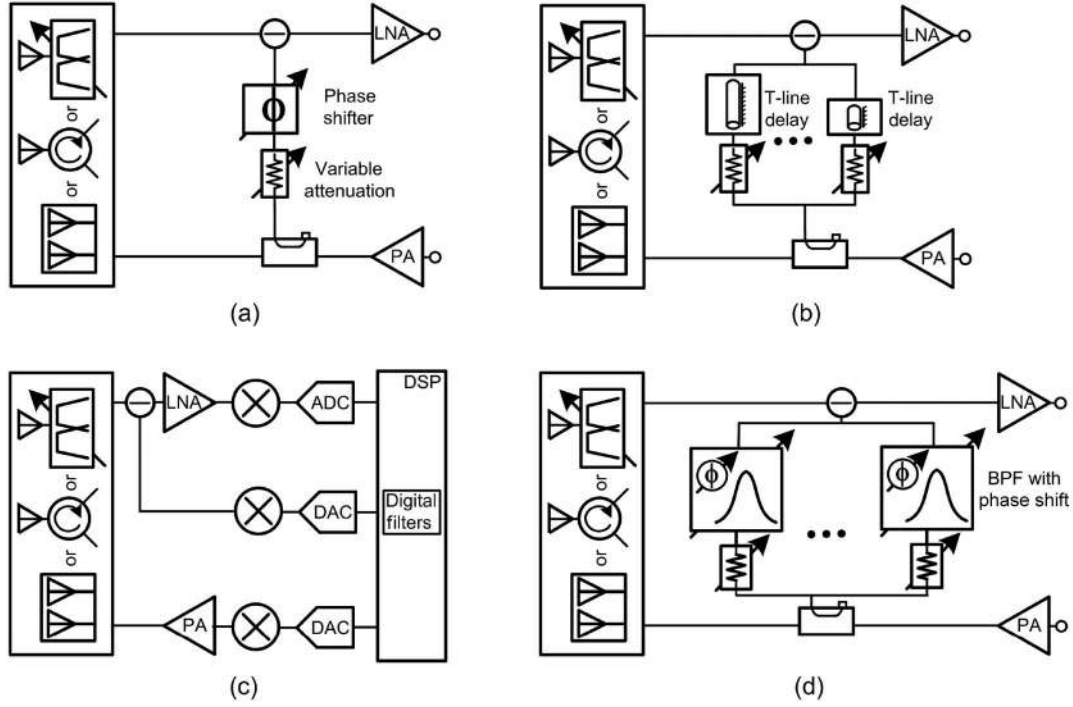
Fig. 2. Approaches for SIC in the RF domain. (a) Conventional frequency-flat amplitude- and phase-based narrowband canceller. (b) Wideband time-domain equalization using true time delays. (c) Wideband mixed-signal cancellation based on digital equalization. (d) Frequency-domain equalization based on BPFs.

analog SIC. Therefore, the ADC dynamic range (DR) is determined by the residual SI, RX distortion, canceller distortion, and RX noise floor ($P_{\text{noise floor}}$) as $\text{DR}_{\text{ADC}} = (P_{\text{TX,main}} - \text{ISO} - \text{SIC}_{\text{RF}} - \text{SIC}_{\text{BB}} + 6) - (P_{\text{noise floor}} - 6)$, where $\text{SIC}_{\text{RF}}$ and $\text{SIC}_{\text{BB}}$ are the amount of SIC achieved in the RF and analog domains, $P_{\text{noise floor}}$ is the RX noise floor ($-174\ \text{dBm/Hz} + 5\ \text{dB} + 73\ \text{dBHz} = -96\ \text{dBm}$), and we have included a 6 dB margin at both ends[2] [6]. Since we have assumed that the RX distortion has the same power as that of the residual SI after RF and analog SIC, we can compute the required RX linearity performance. The RX effective in-band (IB) input-referred third-order intercept point (IIP3) (i.e., IIP3 under RF and analog cancellation of the SI) can be calculated as

$$\text{IIP}_{3,\text{RX,effective}} = (P_{\text{TX,main}} - \text{ISO} - 3)$$
$$+ \frac{1}{2}(\text{SIC}_{\text{RF}} + \text{SIC}_{\text{BB}}). \quad (1)$$

Given 30 dB antenna isolation/cancellation [14], and 50 dB digital SIC [7], 37 dB SIC needs to be achieved in the RF and analog domains, resulting in $\text{DR}_{\text{ADC}} = 56\ \text{dB}$ and $\text{IIP}_{3,\text{RX,effective}} = +0.5\ \text{dBm}$.

One interesting question is how to distribute the 37 dB SIC between RF and analog domains. SIC must be judiciously distributed between the two to ensure that the required $\text{IIP}_{3,\text{RX,effective}}$ is achieved and gain compression and NF increase is prevented along the RX chain. Furthermore, RF SIC at the RX input is required to protect the RX front-end

from cross-modulation distortion [16]. The amount of SIC that can be obtained at RF is also typically limited by the selectivity of the antenna interface and the required RF SIC BW. In this work, through the proposed FDE-based SIC technique in the RF domain, 20 dB cancellation is achieved over >20 MHz BW.[3] Therefore, analog SIC is required to meet the link budget. Preliminary simulations verify that even a frequency-flat analog baseband canceller when co-optimized with our proposed two-filter-based FDE canceller at RF can achieve the required 37 dB SIC across 20 MHz BW.

### B. FD RF SIC Design Requirements and Tradeoffs

The focus of this work is on SIC in the RF domain . Here, we analyze the design tradeoffs associated with the canceller in the RF domain. In Fig. 3, an adjacent channel unknown jammer ($P_{\text{jam}}$) together with SI is present at the RX input. Due to the third-order nonlinearity of the LNA, SI cross-modulates with the jammer generating a distortion signal ($P_{\text{xmod}}$) that cannot be canceled

$$P_{\text{xmod}} = 2(P_{\text{TX,main}} - \text{ISO} - \text{SIC}_{\text{RF}}) + P_{\text{jam}} - 2\text{IIP}_{3,\text{LNA}}$$
$$(2)$$

where $P_{\text{TX,main}}$ is the average power of the two-tone TX signal, and $\text{IIP}_{3,\text{LNA}}$ is the LNA IIP3.[4] To ensure that RX noise floor is

---

[2]The 12 dB margin can account for the addition of the residual SI, RX distortion and canceller distortion for instance.

[3]In works employing frequency-flat amplitude- and phase-based RF cancellers [5], [11], the amount of RF SIC is typically still limited to <27 dB due to amplitude- and phase-resolution considerations.

[4]We assume a current-mode RX implementation so that the mixer following the LNA is highly linear, and that the jammer is filtered out in the analog baseband. Therefore, the LNA is the main source of cross-modulation distortion.
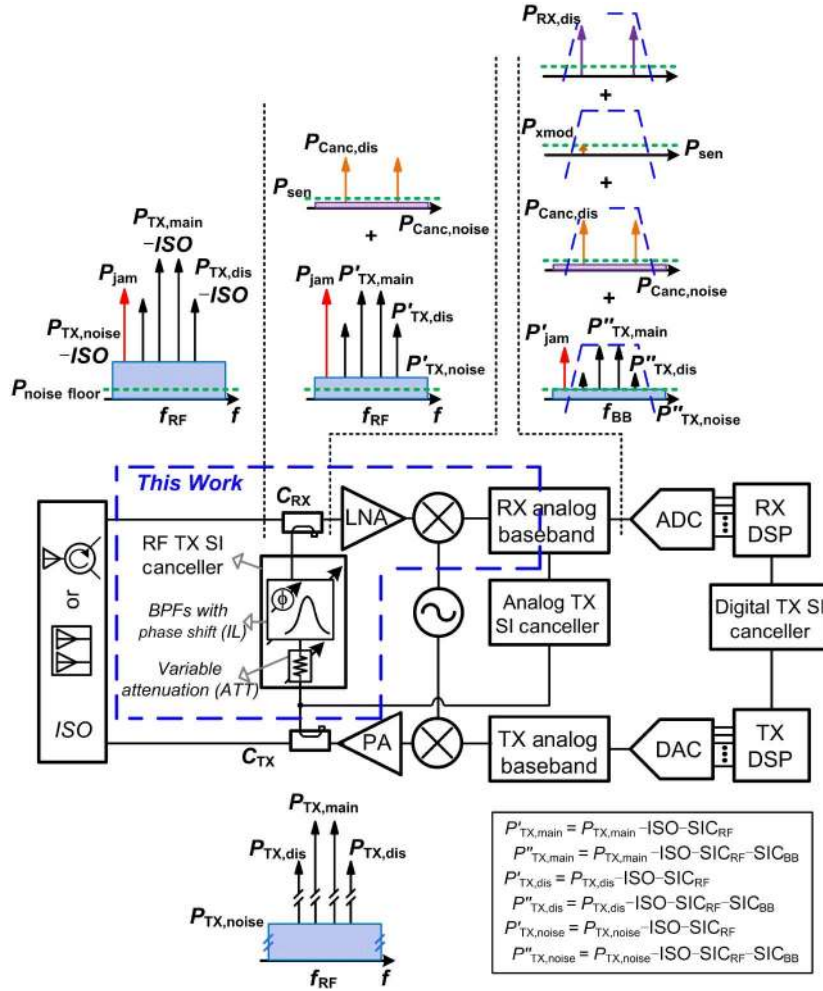
Fig. 3.  FD transceiver block diagram with TX SIC in the RF, analog, and digital domains. Various distortion mechanisms are also depicted.
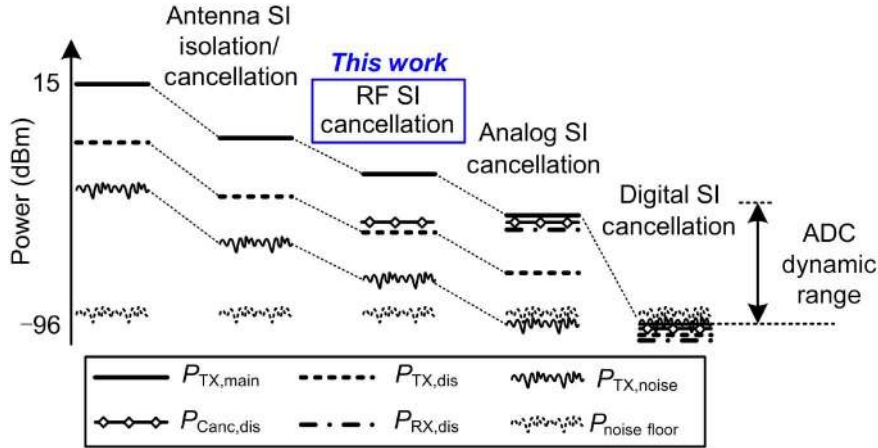


Fig. 4. Link budget of an FD wireless system assuming $+15$ dBm PA output power ($P_{\text{TX,main}}$), 20 MHz RX BW, and 5 dB RX NF. RX noise floor is $P_{\text{noise floor}} = -174\,\text{dBm/Hz} + 5\,\text{dB} + 73\,\text{dBHz} = -96\,\text{dBm}$.

not degraded, the cross-modulation distortion needs to be well below (6 dB below in our calculation) the noise floor, resulting in a required $\text{SIC}_{\text{RF}}$ of

$$\text{SIC}_{\text{RF}} = P_{\text{TX,main}} - \text{ISO} - \text{IIP}_{3,\text{LNA}}$$

$$+ \frac{1}{2}\left(P_{\text{jam}} - P_{\text{noise floor}} + 6\right). \qquad (3)$$

Current-mode RXs typically employ complementary LNTAs that achieve $\text{IIP}_{3,\text{LNA}}$ values around $+10$ dBm. Assume that a conservative $\text{IIP}_{3,\text{LNA}}$ of $+6$ dBm, $P_{\text{TX,main}} = +15$ dBm, $\text{ISO} = 30$ dB, $P_{\text{noise floor}} = -96$ dBm, and $P_{\text{jam}} = -33$ dBm,[5] $\text{SIC}_{\text{RF}}$ of about 14 dB is obtained.

[5]No FD wireless standard is currently available. $P_{\text{jam}}$ is taken from current FDD systems (specifically CDMA [22]).

Regarding the RF canceller's linearity requirement, the third-order intermodulation (IM3) distortion signals ($P_{\text{RX,dis}}$) generated by the canceller are assumed to be at the power level of residual SI after RF and analog SIC (see Fig. 4). Thus, the required OIP3 of the RF canceller is

$$\text{OIP}_{3,\text{Canc}} + \text{CP}_{\text{RX}} = P_{\text{TX,main}} - \text{ISO} - 3$$
$$+ \frac{1}{2}(\text{SIC}_{\text{RF}} + \text{SIC}_{\text{BB}}) \quad (4)$$

where $\text{CP}_{\text{RX}}$ is the coupling strength at the RX side.

In Fig. 3, the RF SI canceller is depicted as consisting of variable attenuators, phase shifters, and reconfigurable BPFs for wideband SIC. Since linearity is typically challenging to achieve in scaled CMOS, one may assume that the variable attenuator precedes the other building blocks in the canceller. Assuming that the noise figure of the BPFs (with embedded phase shifters) is $\text{NF}_{\text{filter}}$, the NF of the RX including the RF canceller can be written as

$$\text{NF}_{\text{RX,tot}} = 10\log_{10}(10^{NF_{\text{RX}}/10} + 10^{(\text{NF}_{\text{filter}}-\text{IL}+\text{CP}_{\text{RX}})/10})$$
$$(5)$$

where IL is the implementation loss of the phase shifter and BPF. Furthermore, the attenuation of the RF canceller and $\text{CP}_{\text{RX}}$ can be related to ISO and the TX-side coupling strength ($\text{CP}_{\text{TX}}$)

$$\text{ISO} = -\text{CP}_{\text{TX}} - \text{CP}_{\text{RX}} + \text{ATT} + \text{IL} \quad (6)$$

where ATT is the attenuation from the variable attenuator. Equations (4)–(6) indicate a design tradeoff between the RX NF degradation and the RF canceller linearity requirement. Assuming $\text{CP}_{\text{TX}} = -10$ dB, ISO $= 30$ dB, $\text{NF}_{\text{RX}} = 5$ dB, IL $= 3$ dB, and $\text{NF}_{\text{filter}} = 15$ dB, canceller OIP3 requirement and RX overall NF including the RF canceller are plotted in Fig. 5 versus $\text{CP}_{\text{RX}}$. The specifications used closely match our implementation described later. For a given ISO, the attenuation that must be achieved in the canceller can be partitioned between ATT and $\text{CP}_{\text{RX}}$ based on (6). $\text{OIP}_{3,\text{Canc}} + \text{CP}_{\text{RX}}$ is fixed based on (4). As shown in Fig. 5, stronger coupling at the RX side relaxes the canceller linearity requirement. Stronger coupling, however, degrades the RX overall NF performance as more canceller noise couples to the RX input as seen in (5). In our design described later, $\text{CP}_{\text{RX}} = -10$ dB is chosen, resulting in canceller OIP3 requirement of 10.5 dBm and an expected NF degradation of less than 2 dB.

The impact of LO phase noise is another important consideration which is beyond the scope of this paper. When separate LOs are used for the TX and RX, LO phase noise can severely limit the overall achievable SIC [23]. In an integrated FD radio, as enabled by our work, a common LO can be shared between TX and RX, and thus phase noise in the TX and RX paths are completely correlated. In such a scenario, the overall achievable SIC is only limited by the delays in the SI channel which reduce the correlation between the transmitted and received SI signal and limit subsequent digital cancellation [23]. RF SIC prior to downconversion in the RX further alleviates this problem and relaxes the LO phase noise requirement.
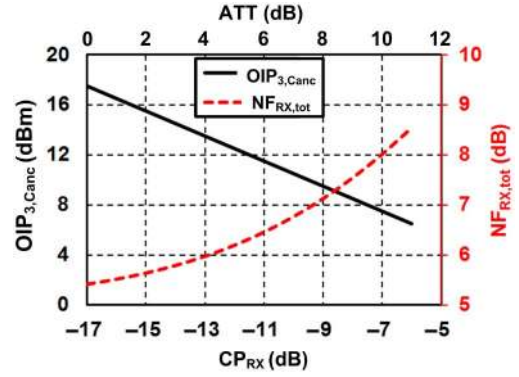


Fig. 5. Canceller output IP3 ($\text{OIP}_{3,\text{Canc}}$) and RX overall NF ($\text{NF}_{\text{RX,tot}}$) including canceller noise versus the coupling strength at the RX side ($\text{CP}_{\text{RX}}$).

Table I summarizes the system-level analysis and specifications presented in this section and compares them to the measurement results described later in this paper.

## III. PROPOSED FDE-BASED WIDEBAND SIC IN THE RF DOMAIN

### A. SIC BW Limitation of a Frequency-Flat RF Canceller

RF SIC BW is typically limited by the frequency selectivity of the antenna interface isolation (such as that of a T/R antenna pair, duplexer, or circulator and including environmental reflections for FD). Fig. 6(a) illustrates an FD transceiver with a conventional frequency-flat RF canceller based on amplitude-and-phase scaling. For simplicity, let us model the antenna interface response [$H_{\text{SI,model}}(j\omega)$] with a flat magnitude response but a constant group delay as $H_{\text{SI,model}}(j\omega) = A_0 \exp(-j(\omega - \omega_0)\tau_{\text{SI}} + j\phi_0)$. $A_0$ is the flat magnitude response, $\tau_{\text{SI}}$ is the isolation group delay, and $\phi_0$ is the phase at frequency $\omega_0$. For the frequency-flat RF canceller, the transfer function (TF) $\hat{H}_{\text{flat}}$ can be written as $\hat{H}_{\text{flat}}(j\omega) = A_C \exp(+j\phi_C)$.[6] $A_C$ and $\phi_C$ are the frequency-flat magnitude and phase responses of the canceller. To achieve RF SIC centered at $\omega_0$, one needs to set $A_C = A_0$ and $\phi_C = \phi_0$. One can then write an equation for the residual SI across $\omega$, and assuming $(\omega - \omega_0)\tau_{\text{SI}} \ll 1$ rad, write an equation for the RF BW ($\omega_{\text{BW}}$) within which the worst-case SIC is $\text{SIC}_{\text{RF}}$. We obtain

$$\omega_{\text{BW}} = \frac{2}{\sqrt{\text{SIC}_{\text{RF}}}\tau_{\text{SI}}}. \quad (7)$$

$\text{SIC}_{\text{RF}}$ is plotted versus $f_{\text{BW}}$ in Fig. 6(b) for $\tau_{\text{SI}} = 1$, 10, and 25 ns. For $\text{SIC}_{\text{RF}} = 20$ dB, the supported SI RF BWs are 31, 3, and 1.2 MHz, respectively.

Fig. 6(c) plots the measured isolation TF[7] of a 1.4 GHz antenna pair (see Fig. 24) $H_{\text{SI}}(j\omega)$ with 32 dB peak TX/RX isolation, 9 ns peak isolation group delay, and 3 dB isolation

---

[6]The hat above the TF is used to signify a canceller that is attempting to approximate an antenna interface.

[7]To obtain this isolation TF, the antenna pair $S$-parameters are first measured. Using the measured $S$-parameters, the RX port output current is simulated with a short-circuit termination at the RX port The short represents the virtual ground created by SIC at the RX port. The isolation TF is then computed by multiplying the short-circuit output current by the reference resistance.

TABLE I
SUMMARY OF THE SPECIFICATIONS FOR AN FD SYSTEM AND CORRESPONDING MEASUREMENT RESULTS

| | | Specifications | | Measurement results |
|---|---|---|---|---|
| | | Requirements | Comments | |
| System definition | $P_{TX,main}$ (TX output power) | +15 dBm | | +15 dBm[a] |
| | Self-interference (SI) bandwidth | 20 MHz | BW for LTE [1] | >20 MHz[b] |
| | $NF_{RX}$ (RX NF without SIC) | 5 dB | | 4.8–5.8 dB |
| | $P_{noise floor}$ (RX noise floor) | −96 dBm | Calculated from $NF_{RX}$ and BW | −96.2 to −95.2 dBm |
| | $P_{jam}$ (CW jammer power) | −33 dBm | Referred from CDMA standard [22] | −33 dBm |
| | Total SI cancellation (SIC) | 117 dB | To suppress SI 6 dB below RX noise floor | 52 dB over 27 MHz (ISO + RF SIC)[i] |
| SIC budget | ISO (antenna isolation) | 30 dB | | 32 dB[c] |
| | $SIC_{RF}$ | 20 dB | Determined by (3) and SIC BW | 20 dB over 27 MHz SI BW[i] |
| | $SIC_{BB}$ | 37 dB − $SIC_{RF}$ | Assuming 117 dB required total SIC, 30 dB ISO and 50 dB $SIC_{digital}$ | Not implemented |
| | $SIC_{digital}$ | 50 dB | Based on [7] | Not implemented |
| | SI delay $\tau_{SI}$ (SI delay from the direct coupling path) | 10 ns | | 9 ns[c] |
| Circuit performance | $DR_{ADC}$ | 56 dB | Determined by $DR_{ADC} =$ ($P_{TX},main$–ISO–$SIC_{RF}$–SICBB+6) −($P_{noise floor}$-6) | Not implemented |
| | In-band IIP3.RX,effective (RX IIP3 with respect to SI under SIC) | +0.5 dBm | Determined by (1) | +2 dBm[e] |
| | IIP3.LNA | +6 dBm | Typical value for LNTA. | +17 dBm[f] |
| | $CP_{TX}$ (coupling strength at TX side) | −10 dB | 10% reduction of TX efficiency | −10 dB |
| | $CP_{RX}$ (coupling strength at RX side) | −10 dB | Determined by (4)–(6) | −10 dB[d] |
| | OIP3,Canc (canceller OIP3) | +10.5 dBm | Determined by (4) | N/A[h] |
| | $NF_{filter}$ (canceller filter noise figure) | 15 dB | From filter implementation. | 16 dB[d] |
| | NF degradation under RF SIC | < 2 dB | Determined by (5) | 1.1–1.3 dB |
| | ATT+IL (total attenuation or loss from the canceller in the RF domain) | 10 dB | Determined by (6) | 12B[g] |

[a]Transmitted power in the RF SIC demonstration measurement shown in Fig. 24. This is also the transmitter power at which other table parameters are reported. Note that higher levels of SI can be canceled at the RX input assuming ISO = 30 dB.
[b]Maximum achieved 20 dB RF SIC BW in Fig. 20(b) is 25 MHz and the wireless demonstration in Fig. 24 uses 27 MHz.
[c]This represents the peak isolation magnitude and group delay of the 1.4 GHz antenna pair's direct coupling path.
[d]Based on the simulations of the design.
[e]Includes canceller IM3 distortion as well.
[f]Estimated from RX OOB IIP3 measurement.
[g]Calculated as $ISO + CP_{TX} + CP_{RX} = 32 - 10 - 10$ dB = 12 dB.
[h]Canceller IM3 distortion is included in the measured in-band effective IIP3 ($IIP_{3,RX,effective}$).
[i]From the wireless demonstration in Fig. 24.

magnitude variation over 1.36–1.38 GHz. The TF of a frequency-flat amplitude- and phase-based RF canceller is also plotted in Fig. 6(c). The conventional RF canceller can only emulate the frequency selective antenna interface at a single cancellation frequency, resulting in a 20 dB SIC BW of about 3 MHz in Fig. 6(c). This matches very well with the result in (7).

### B. SIC Based on RF Frequency-Domain Equalization

To enhance the cancellation BW, second-order reconfigurable BPFs with amplitude and phase control in each path are introduced in the RF canceller [Fig. 7(a)]. The reconfigurable BPFs can be modeled using a second-order RLC BPF as shown in Fig. 8, where transconductance $g_i$ and phase $\phi_i$ present the amplitude and phase control in the $i$th path. The
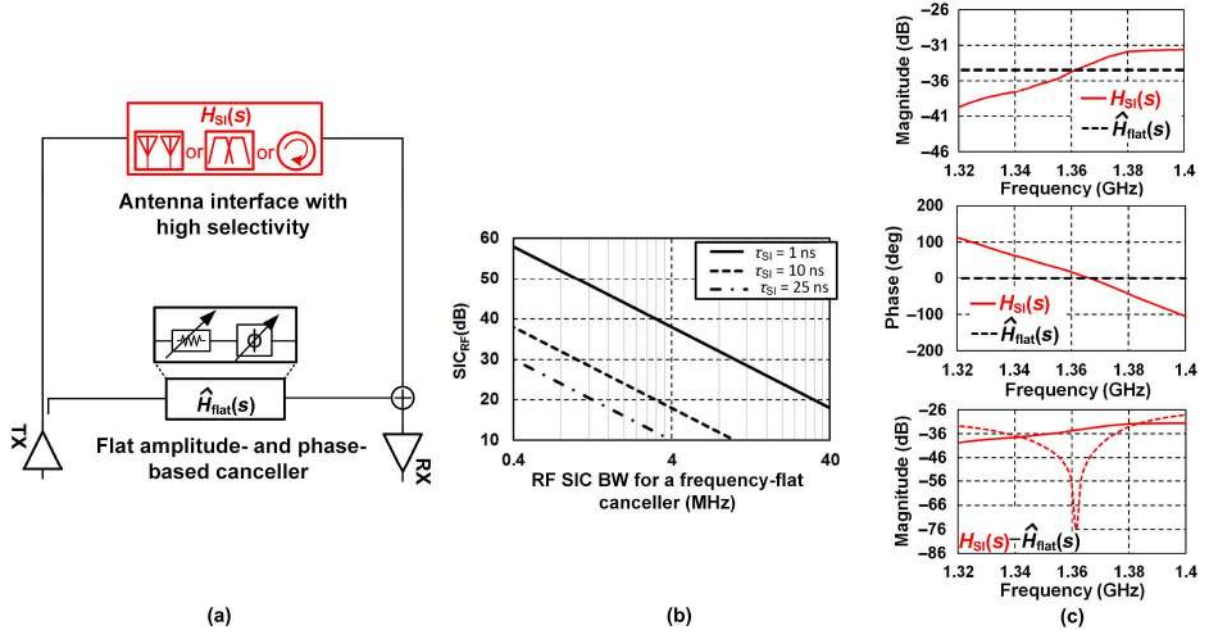
Fig. 6. Conventional frequency-flat RF canceller based on amplitude and phase scaling. (a) Block diagram. (b) Calculated RF SIC BW for a given worst-case $SIC_{RF}$ for a frequency-flat amplitude- and phase-based canceller using (7) across various SI channel delays. (c) Frequency responses of an antenna interface and the RF canceller and the resultant SIC. Measured isolation TF of a 1.4 GHz antenna pair (see Fig. 24) is used for $H_{SI}(s)$.
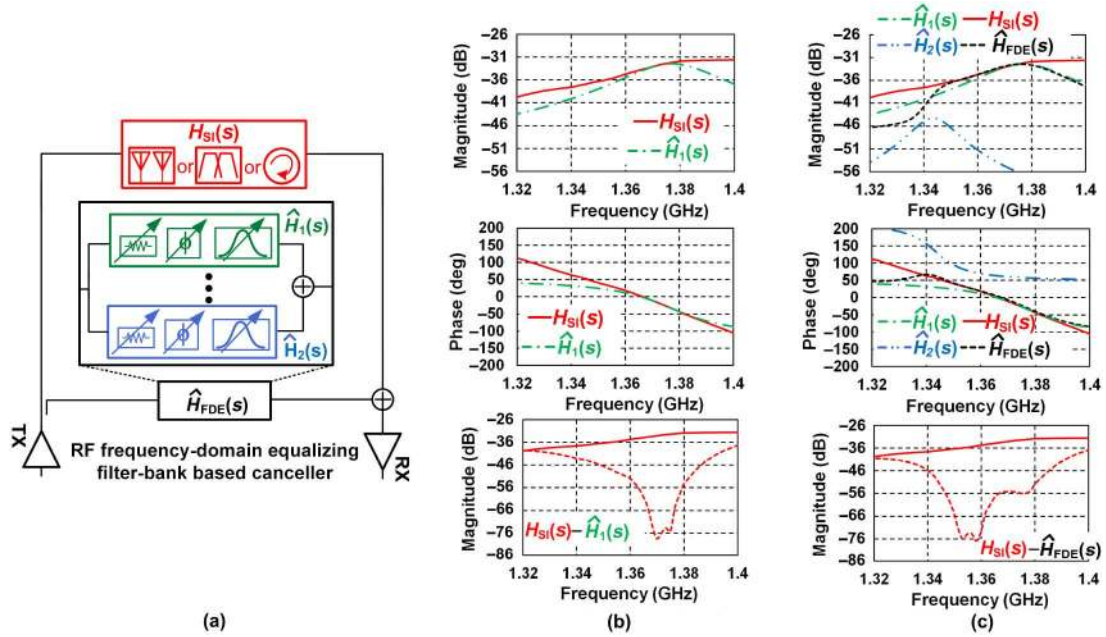


Fig. 7. Proposed RF canceller based on FDE. (a) Block diagram. (b) Frequency responses of the antenna interface and the RF canceller with one filter and the resultant SIC. (c) Frequency responses of the antenna interface and the RF canceller with two filters and the resultant SIC. The $H_{SI}(s)$ is the same as in Fig. 6. The TFs of the canceller filters $\hat{H}_1$ and $\hat{H}_2$ follow (8). The canceller filter settings are mentioned in the text.

short termination at the canceller output represents the virtual ground created by SIC. The TF of the $i$th path is

$$\hat{H}_i(j\omega) = \frac{A_i \, \exp(-j\phi_i)}{1 - jQ_i\frac{\omega_i}{\omega}\left(1 - \frac{\omega^2}{\omega_i^2}\right)} \qquad (8)$$

where $Q_i = \frac{R||R_{p,i}}{\omega_i L_i}$ represents the quality factor, $\omega_i = 1/\sqrt{L_i C_i}$ is the center frequency, and $A_i = \frac{g_i R_{p,i}}{R_{p,i}+R}$ and $\phi_i$ are

the magnitude and phase settings of the $i$th BPF, respectively. *Thus, an RF canceller with a reconfigurable second-order RF BPF features four degrees of freedom ($A_i$, $\phi_i$, $Q_i$, and $\omega_i$) and enables the replication of not just the magnitude and phase of the antenna interface isolation at a frequency point, but also the slope of the magnitude and the slope of the phase (or group delay),* enhancing the 20 dB SIC BW from 3 to 19 MHz as shown in Fig. 7(b). As shown in the appendix, the
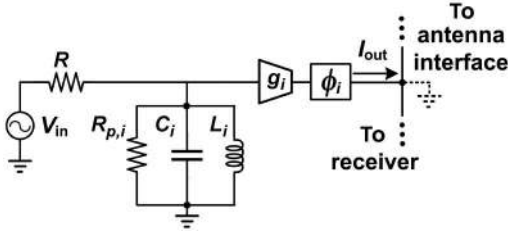
Fig. 8. Equivalent second-order RLC BPF model for the BPF in Fig. 7(a). Transconductance $g_i$ and phase $\phi_i$ represent the amplitude and phase control, respectively. The short termination at the canceller output represents the virtual ground created by SIC.

BPF parameters can be solved based on the antenna interface response $[H_{\mathrm{SI}}(j\omega)]$

$$\phi_i = \angle H_{\mathrm{SI}}(j\omega_{\mathrm{SIC},i}) + \arctan\frac{B}{|H_{\mathrm{SI}}(j\omega_{\mathrm{SIC},i})|} + \pi,$$

$$\omega_i = \sqrt{\frac{1+P}{1-P}}\,\omega_{\mathrm{SIC},i},$$

$$Q_i = -\frac{B}{|H_{\mathrm{SI}}(j\omega_{\mathrm{SIC},i})|}\frac{1+P}{2P}\frac{\omega_{\mathrm{SIC},i}}{\omega_i},$$

$$A_i = \sqrt{1 + K(\omega_{\mathrm{SIC},i})^2}\,|H_{\mathrm{SI}}(j\omega_{\mathrm{SIC},i})| \qquad (9)$$

where $\omega_{\mathrm{SIC},i}$ is the cancellation frequency for the $i$th BPF, and $B$, $P$, and $K$ are shorthand notations defined in the appendix. In Fig. 7(b), $\omega_{\mathrm{SIC},1}$ is chosen to be $2\pi \times 1.370\,\mathrm{Grad/s}$. Based on (9), $\omega_1 = 2\pi \times 1.377\,\mathrm{Grad/s}$, $Q_1 = 40.6$, $A_1 = -32.4$ dB, and $\phi_1 = -33.3°$.

The use of a filter bank with independent BPF parameters enables such replication at multiple points in different sub-bands, further enhancing SIC BW. In Fig. 7(c), the use of two filters enhances the 20 dB SIC BW to 32 MHz, respresenting a $10\times$ improvement over a conventional RF canceller. *Essentially, this approach is FDE in the RF domain.* An iterative successive cancellation approach is used for SIC in Fig. 7(c): $\hat{H}_1$ first emulates the antenna interface $H_{\mathrm{SI}}$ at $\omega_{\mathrm{SIC},1} = 2\pi \times 1.370\,\mathrm{Grad/s}$, then $\hat{H}_2$ replicates the residual response $(H_{\mathrm{SI}} - \hat{H}_1)$ at $\omega_{\mathrm{SIC},2} = 2\pi \times 1.350\,\mathrm{Grad/s}$. Since the introduction of $\hat{H}_2$ will adversely affect the cancellation originally achieved at $\omega_{\mathrm{SIC},1}$, iteration of $\hat{H}_1$ and $\hat{H}_2$ is required. In Fig. 7(c), the filter parameters calculated using (9) in an iterative successive fashion are $\omega_1 = 2\pi \times 1.377\,\mathrm{Grad/s}$, $Q_1 = 40.6$, $A_1 = -32.4$ dB, $\phi_1 = -33.3°$, $\omega_2 = 2\pi \times 1.343\,\mathrm{Grad/s}$, $Q_2 = 81.2$, $A_2 = -44.2$ dB, and $\phi_2 = 133.3°$.

### C. Two-Port N-Path Canceller Filter

As shown in Section III-B, reconfigurable BPFs with high quality factor (e.g., as high as 81.2 in the example shown in Fig. 7), amplitude control, and phase shifting functionality are required. Recently, N-path filters [18] have emerged as a promising solution for the implementation of integrated widely tunable high-$Q$ RF filters [19], [20]. In this paper, we propose a two-port N-path $G_m$-C filter with embedded variable attenuation and phase shifting.

Fig. 9(a) depicts a two-port $N$-path filter, where $R_S$ and $R_L$ are the resistive loads at the TX and RX sides, respectively. $C_C$ weakly couples the cancellation signal to the RX input for SIC. The quality factor of an $N$-path filter may be reconfigured via the baseband capacitor $C_B$, given fixed $R_S$ and $R_L$. Linear periodic time-variant (LPTV) analysis yields [24]

$$Q = 4\pi f_S[(R_S + R_{\mathrm{on}})||(R_L + R_{\mathrm{on}})]C_B \qquad (10)$$

where $R_{\mathrm{on}}$ is the on-resistance of the $N$-path switches, $f_S$ is the switching frequency, and we have ignored the loading effect of $C_C$. Through clockwise/counter-clockwise (only counter-clockwise connection is shown in Fig. 9(a) for simplicity)-connected baseband reconfigurable transconductors ($G_m$), an upward/downward frequency offset with respect to the switching frequency can be obtained [21]. The frequency offset of the center frequency to the switching frequency is given by $\Delta\omega = \frac{G_m}{C_B}$ [21]. Variable attenuation can be introduced by reconfiguring $R_S$ and $R_L$ relative to each other [Fig. 9(b)]. The magnitude response at the center frequency is

$$|H(j\omega_S)| = \left|\frac{I_{\mathrm{canceller}}}{V_{\mathrm{in}}}\right|_{\omega=\omega_S} R_0 = \left|\frac{V_{\mathrm{out}}}{V_{\mathrm{in}}}\right|_{\omega=\omega_S}$$

$$\times \omega_S C_C R_0 \approx \frac{8}{\pi^2}\frac{(R_L + R_{\mathrm{on}})\omega_S C_C R_0}{R_S + R_L + 2R_{\mathrm{on}}} \qquad (11)$$

where we have ignored the loading effect of $C_C$ when calculating $V_{\mathrm{out}}$. It should be noted that once cancellation is performed, $V_{\mathrm{RX}}$ is a virtual ground. The canceller TF is computed by finding the $I_{\mathrm{canceller}}$ that flows into the virtual ground and multiplying it by the reference resistance $R_0$. Also, in (11), the center frequency is assumed to be $\omega_S$, i.e., $G_m = 0$, for simplicity.

*Interestingly, phase shifting can be embedded in a two-port N-path filter by phase shifting the LOs driving the switches on the output side as in Fig. 9.* A complete LPTV analysis of a two-port $N$-path filter with embedded phase shifting is mathematically involved. While beyond the scope of this paper, we have completed this analysis elsewhere [25]. The analysis in [25] reveals that phase shifting the LOs driving the output-side switches imparts constant phase shifts to the two-port $N$-path filter frequency response with no other impact on close-in response. Fig. 10 plots the simulated magnitude and phase responses of the two-port $N$-path filter shown in Fig. 9(a) with embedded phase shifting. In simulation, 25% non-overlapping LOs are used with $R_{\mathrm{on}} = 3.3\ \Omega$, $R_S = R_L = 50\ \Omega$, $C_B = 200$ pF, $C_C = 0$ pF. All $G_m = 0$ S and do not load the $N$-path filter.

## IV. CIRCUIT IMPLEMENTATION

A canceller bank of two reconfigurable second-order $G_m$-C $N$-path filters together with a 0.8–1.4 GHz reconfigurable current-mode RX is implemented in a 65 nm standard CMOS process. The block diagram is shown in Fig. 11. The canceller filters have separate LO and TX replica signal inputs, lending flexibility in their use (e.g., cancellation of two separate TX signals for MIMO applications). The RX uses
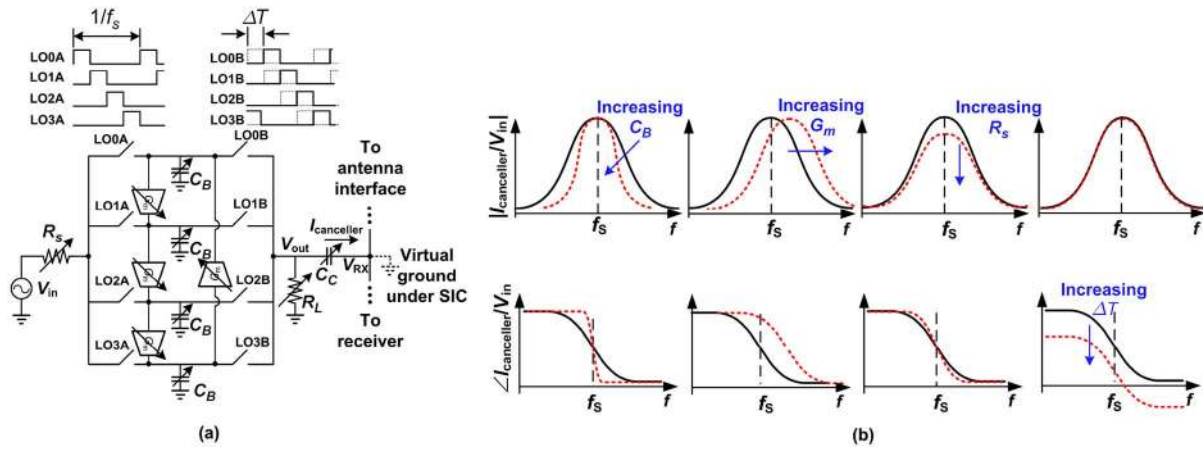
Fig. 9. Two-port $G_m$-$C$ $N$-path filter implementation with embedded variable attenuation and phase shift. (a) Block diagram. (b) Illustration of variable quality-factor (group delay), frequency shift, attenuation, and phase shift.
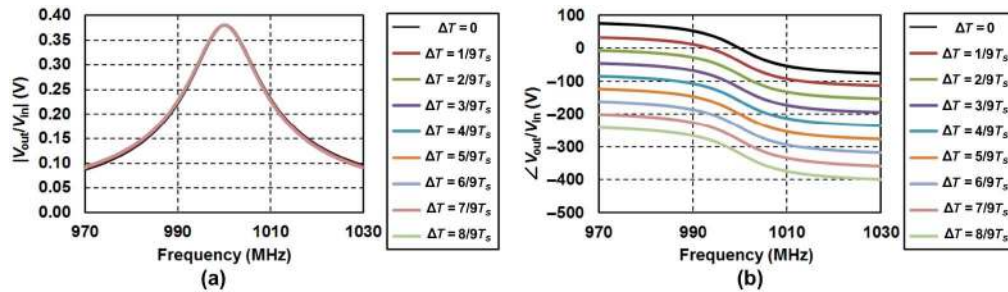


Fig. 10. Simulated (a) magnitude and (b) phase responses of the two-port $N$-path filter shown in Fig. 9(a). In simulation, ideal 25% non-overlapping LOs drive ideal $N$-path switches with $R_{on} = 3.3\ \Omega$, $R_S = R_L = 50\ \Omega$, $C_B = 200$ pF, and $C_C = 0$ pF. All $G_m = 0\ S$ and do not load the $N$-path filter.
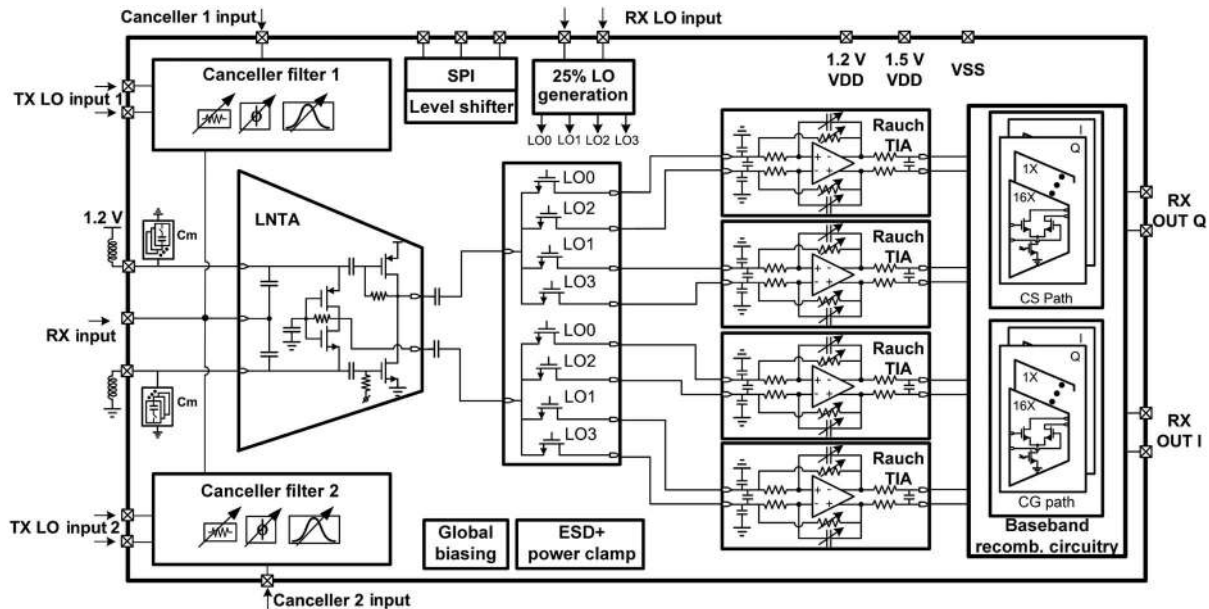


Fig. 11. Block diagram and schematic of the implemented 0.8–1.4 GHz 65 nm CMOS RX with FDE-based SIC in the RF domain featuring a bank of two filters.

a noise-canceling common-gate (CG), common-source (CS) low-noise transconductance amplifier (LNTA) followed by 4-phase current-driven passive mixers and baseband TIAs [16]. Programmable baseband recombination circuits combine the RX outputs from the CG and CS paths for noise cancellation [16], [26].

For each canceller filter as illustrated in Fig. 12, the coupling capacitor $C_C$ bank is designed to enable a $-10$ dB coupling across the operating frequency range based on our discussion in Section II-A. In addition, a relatively weak coupling is important for SIC at the RX input to not degrade the RX input matching as well as to prevent $N$-path filters from interacting
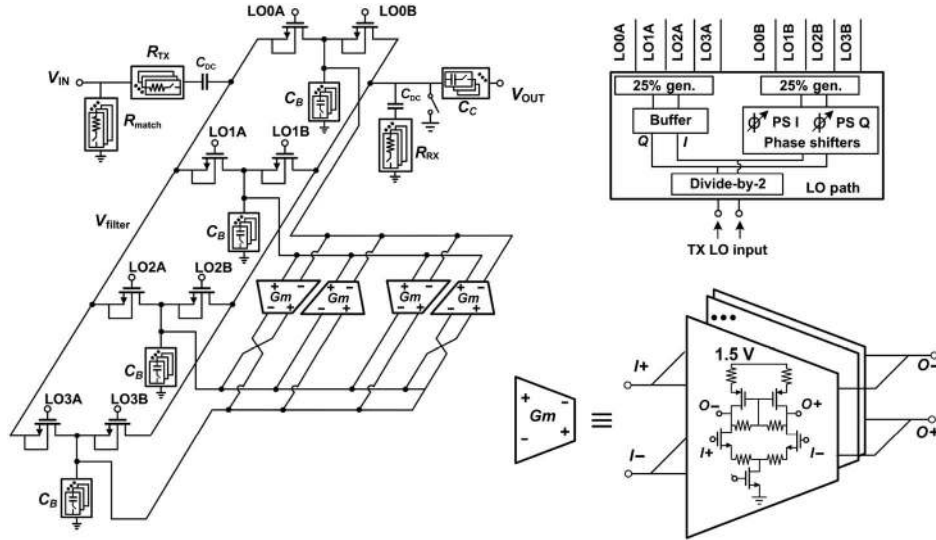
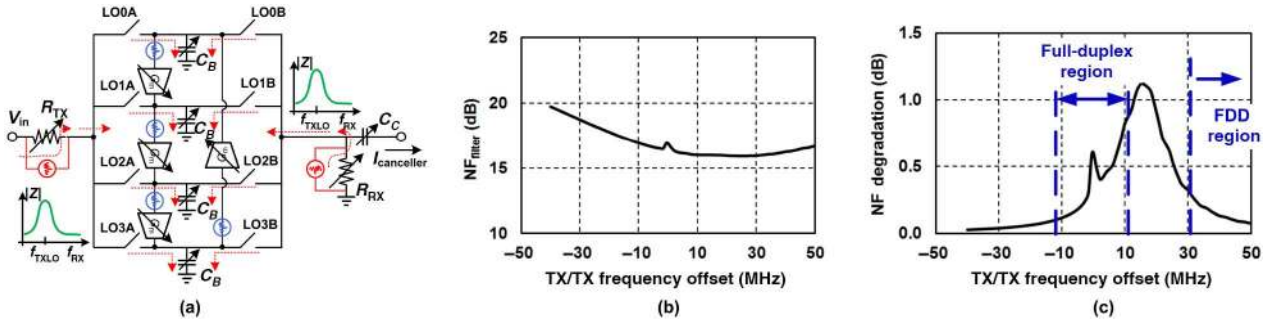Fig. 12. Block diagram and schematic of each canceller filter.



Fig. 13. (a) Illustration of noise filtering for FDD. (b) Simulated canceller filter noise figure $NF_{filter}$. (c) RX NF degradation due to one canceller filter assuming $NF_{RX} = 6$ dB. To obtain the $NF_{filter}$, the attenuation that precedes the filter input has been simulated and de-embedded. ($R_{TX} = R_{RX} = 50\ \Omega$, $R_{match} = 60\ \Omega$, $C_B = 200$ pF, $G_m = 26$ mS, $C_C = 2.5$ pF, $f_S = 1$ GHz, resulting in a total attenuation of about 20 dB including RX-side coupling, frequency shift of 15 MHz, phase shift of $0°$, and $Q$ of about 67.)

with each other and with the RX. Next, $R_{RX}$ (nominal value 50 $\Omega$) is sized to be smaller than $|\omega C_C|^{-1}$, so that the capacitive loading effect of $C_C$ on the $N$-path filter is weak. Based on the required attenuation range and (11), the resistance range of $R_{TX}$ can be obtained. Once $R_{TX}$ and $R_{RX}$ are set, using (10), the $N$-path filter baseband capacitance range is determined by the required group delay or quality-factor range. Finally, the transconductance range of the baseband $G_m$ is designed using $\Delta\omega = \frac{G_m}{C_B}$ based on the required frequency shift range as well as the $C_B$ capacitance range. Based on the aforementioned design principles, both canceller filters are designed to have a digitally controlled peak group delay that ranges from 1 to 28 ns, a frequency shift that ranges from $-10$ to $+10$ MHz under the peak group delay setting, full $360°$ phase shift range, and an attenuation range from 20 to 40 dB including the 10 dB RX-side capacitive coupling. The capacitive load present at the RX input due to the capacitive coupling is resonated out using a combination of wirebond and off-chip inductance. Furthermore, programmable capacitor banks ($C_m$) are included to tune the input match to the desired frequency.

The schematic of the $G_m$ cells is shown in Fig. 12. To ensure a high canceller linearity, the $G_m$ cells of the canceller filters are source-degenerated and operate under slightly higher supply

voltage (1.5 V) than the rest of the chip (1.2 V). In addition, the on-resistance ($R_{on}$) of the $N$-path switches is designed to be 3.3 $\Omega$ (much smaller than $R_{TX}$ and $R_{RX}$), so that its impact on overall canceller linearity is minimized. Linearity simulations of the canceller filters (and $N$-path filters in general) are challenging due to discontinuities in the higher order derivatives of drain current and terminal charges in BSIM models for MOSFET devices operating as switches [27]. Measurements of IB RX effective IIP3 under cancellation of FD SI described in the following section confirm that the IM3 distortion of the canceller filters remains within the performance specifications discussed in Section II-B.

An interesting benefit for FDD applications of using a frequency-selective reciprocal canceller is noise-filtering. In this work, for FDD, we target the cancellation of the powerful main SI signal in the TX band at the RX input. Cancellation of the TX noise in the RX band can be performed later in the RX chain [16] or even in the digital domain [28]. Since the filter banks are tuned to the TX frequency, the RX band noise of $R_{TX}$, $G_m$ cells and even $R_{RX}$ will be filtered by the low RX-band impedance of the $N$-path filter [see Fig. 13(a)]. Using the canceller filter settings annotated in the caption, the simulated canceller filter noise figure $NF_{filter}$ and RX NF
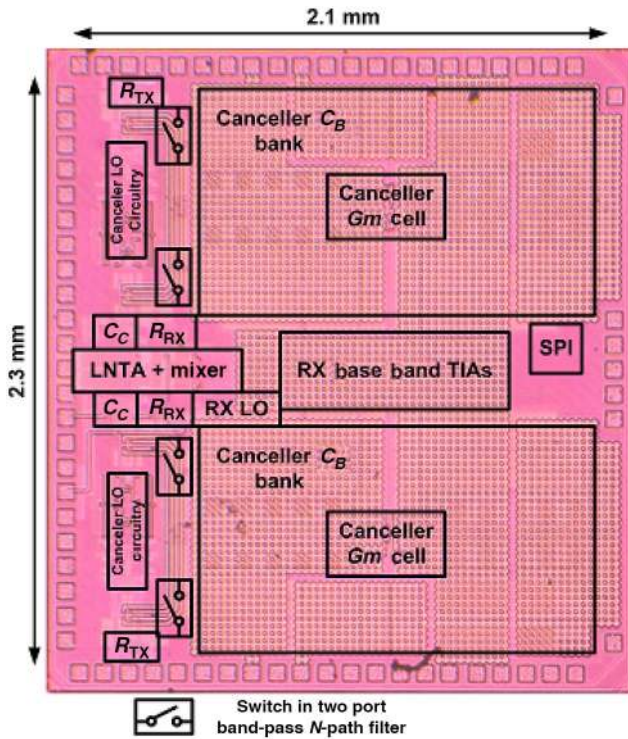
Fig. 14. Chip microphotograph of the 65 nm CMOS 0.8–1.4 GHz SI-canceling RX.

degradation (given $NF_{RX} = 6$ dB) is shown in Fig. 13(b) and (c). To obtain the $NF_{filter}$, the attenuation that precedes the filter has been simulated and de-embedded. As shown in Fig. 13(c), for TX/RX frequency offset >30 MHz, the NF degradation is less than 0.3 dB. NF degradation for TX/RX frequency offsets between −10 and +10 MHz ranges from 0.1 to 0.8 dB and the maximum NF degradation is only slightly higher than 1 dB, thanks to the weak coupling at the RX side. In addition, the $G_m$ cells use channel length of 200 nm to lower the flicker noise.

The LO path of each filter includes a divide by two quadrature divider, LO slew-rate-control filters, I/Q vector-interpolation phase shifters, and 25% duty-cycle generators. The slew-rate-control RC filters attenuate the harmonics to ensure the linearity of the subsequent vector interpolators.

## V. MEASUREMENT RESULTS

The chip microphotograph is shown in Fig. 14 and has an active area of $4.8\,mm^2$. The chip is wire bonded and packaged in a QFN package, and mounted on a PCB for all measurements.

### A. RX Without SIC

Basic RX measurements are performed with the canceller inactive and without SI. The RX has a measured programmable conversion gain that ranges from 27 to 42 dB. The measured RX noise figure [Fig. 15(a)] ranges from 4.8 to 5.8 dB over the operating frequency range. The RX has a measured out-of-band (OOB) and IB IIP3 of +17 and −20 dBm, respectively [Fig. 15(b)]. The measured RX OOB and IB blocker-induced

1 dB gain compression points (blocker P1 dB) are +4 and −30 dBm, respectively.

### B. SIC With a 30 dB TX/RX Isolation Duplexer for FDD

For FDD, the SI canceller enables the usage of a custom-designed LTE-like duplexer employing surface-mount-device-based second-order LC filters with TX band isolation as small as 30 dB, which is 25 dB relaxed compared to commercial SAW/FBAR duplexers [29]. The TX and RX 1 dB BWs are 762–798 MHz and 872–918 MHz (Fig. 16). The highly selective duplexer has a peak isolation group delay of 11 ns and 7 dB magnitude variation across the TX band.

An iterative successive cancellation approach as described in Section III-A is used for canceller calibration.[8] The measured TX/RX isolation with SIC is shown in Fig. 17. The SI canceller achieves a 20 dB cancellation BW of 17/24 MHz for one/two filters enabled, while a conventional frequency-flat amplitude-and-phase-based canceller has a 20 dB SIC BW of only 3 MHz. Note that in measurement, the two canceller filters share the same LO, namely the TX LO frequency which is set at the center of the TX band, and the $G_m$ cells are used to impart frequency shifts.

The associated NF increase is only 0.5/0.6 dB due to noise filtering (Fig. 18), as the NF degradation is lower in the FDD region, i.e., in the vicinity of the RX frequency than in the vicinity of the TX frequency. In measurement, SIC of up to −4 dBm of peak OOB TX leakage at the RX input is demonstrated. The SIC enhances the RX effective OOB IIP3 from +17 dBm to +25 to +27 dBm from cross-modulation (triple-beat) measurements [Fig. 19(a)] and OOB IIP2 from +61 dBm to an effective +90 dBm [Fig. 19(b)]. To be fair, we ensure that the two-tone TX signal undergoes a cancellation of not more than 25 dB (the average cancellation over the 24 MHz 20 dB SIC BW).

### C. SIC Across an Antenna Pair for FD Wireless

For same-channel FD, we use a 1.4 GHz narrowband antenna-pair interface with peak isolation group delay of 9 ns, peak isolation magnitude of 32,[9] and 3 dB of isolation magnitude variation over 1.36–1.38 GHz. Please note that this is the same antenna interface assumed for the analyses presented in Sections III-A and III-B. The SI canceller achieves a 20 dB cancellation BW of 15/25 MHz (one/two filters) in Fig. 20. When a conventional frequency-flat amplitude- and phase-based canceller is used, the SIC BW is about 3 MHz. Once again, in measurement, the two canceller filters share the same LO.

The associated NF increase is 0.9–1.1 dB/1.1–1.3 dB (Fig. 21). Measured RX gain imparted to a weak desired signal without and with SIC are shown in Fig. 22. SIC of up to −8 dBm of peak IB SI at the RX input results in negligible gain

---

[8]The calculated parameters using (9) are used as initial settings. Subsequent manual tuning is used for optimal SIC BW.

[9]More than 30 dB antenna isolation is achieved through physical separation here, but can also be obtained through antenna cancellation in practice [8], [14]. It should be noted that the 9 ns group delay significantly exceeds the delay associated with the physical separation (about 0.4 m) due to the tuned nature of the antennas.
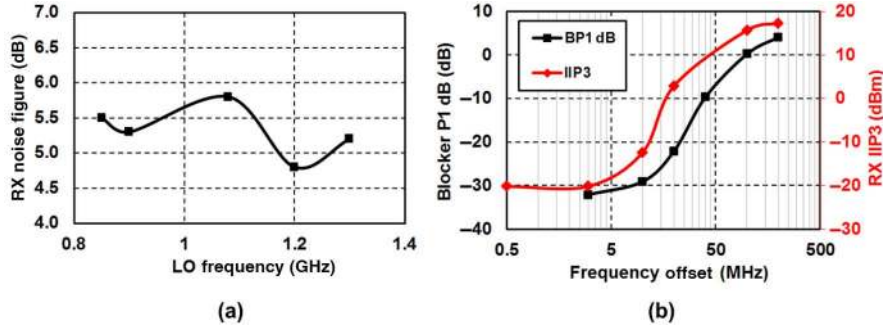
Fig. 15. Measured RX performance with canceller inactive and without SI. (a) Noise figure. (b) IIP3 and blocker-induced 1 dB compression point. IIP3 is plotted versus the frequency offset of the first tone in the two-tone test.
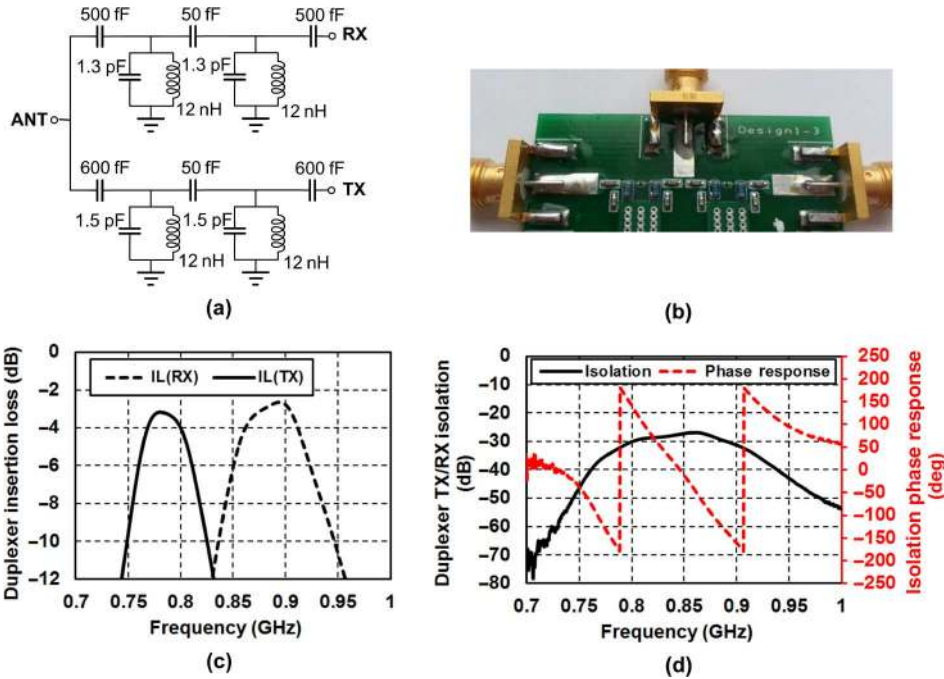


Fig. 16. Custom-designed LTE-like 0.780/0.895 GHz duplexer employing surface-mount-device-based second-order LC filters: (a) schematic; (b) duplexer photo; (c) measured duplexer insertion loss; and (d) measured duplexer TX/RX isolation magnitude and phase response.
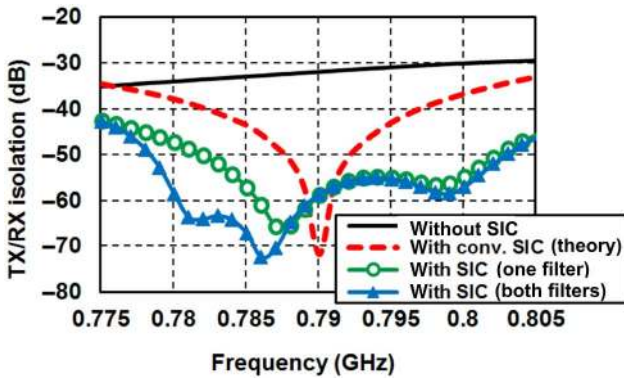


Fig. 17. Measured TX/RX isolation of the FDD LTE-like duplexer shown in Fig. 16 without SIC, and with the proposed SIC. The proposed SI canceller achieves a 20 dB cancellation BW of 17/24 MHz for one/two filters enabled, while a conventional frequency-flat amplitude- and phase-based canceller has a theoretical 20 dB SIC BW of only 3 MHz.
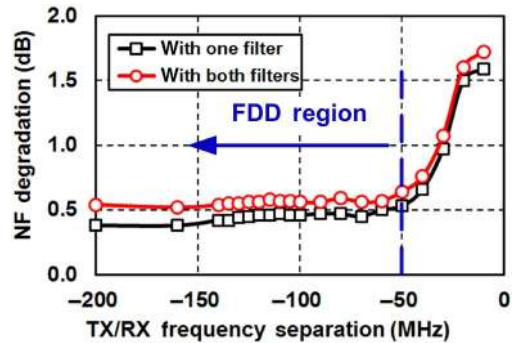


Fig. 18. Measured RX NF degradation with one/two filters enabled versus TX/RX frequency offset. In other words, the RX LO frequency is swept with respect to the TX LO frequency used for the cancellers. Canceller settings for the FDD SIC measurement in Fig. 17 are used.
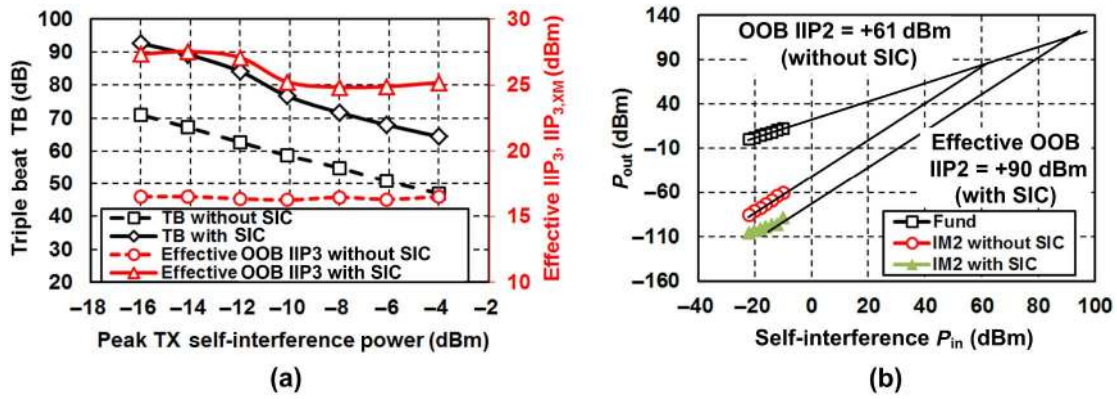
Fig. 19. FDD linearity measurement: (a) TB and (b) IIP2 measurements with and without SIC with a two-tone OOB SI of varying power. For TB measurement, a −33 dBm IB CW jammer is present at the RX input. To be fair, we ensure that the two-tone TX signal undergoes a cancellation of not more than 25 dB for these measurements (the average cancellation over the 24 MHz 20 dB SIC BW in Fig. 17).
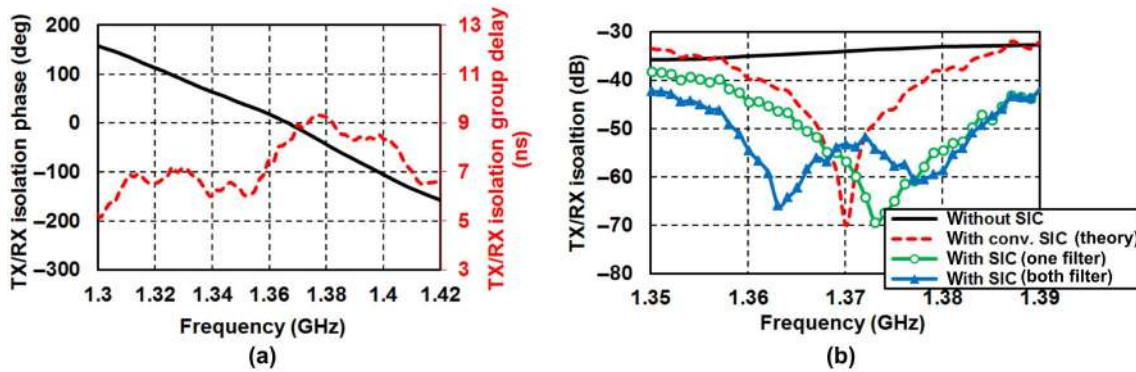


Fig. 20. Measured TX/RX isolation of the 1.4 GHz FD antenna pair shown in Fig. 24 with and without the proposed SIC. (a) TX/RX isolation phase and group delay. (b) TX/RX isolation magnitude without SIC, with conventional SIC (theoretical), and with the proposed SIC. The proposed SI canceller achieves a 20 dB cancellation BW of 15/25 MHz for one/two filters enabled, while a conventional frequency-flat amplitude- and phase-based canceller has a 20 dB SIC BW of only 3 MHz.
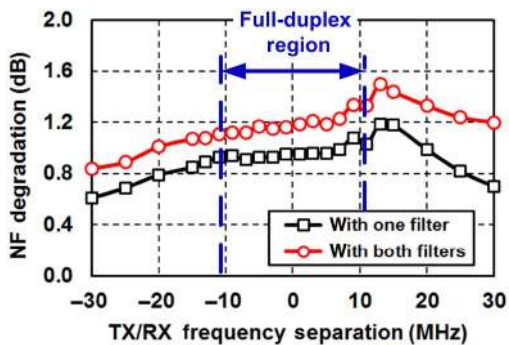


Fig. 21. Measured RX NF degradation with one canceller filter and both canceller filters enabled versus TX/RX frequency offset. Canceller settings for the same-channel FD SIC measurement in Fig. 20 are used.
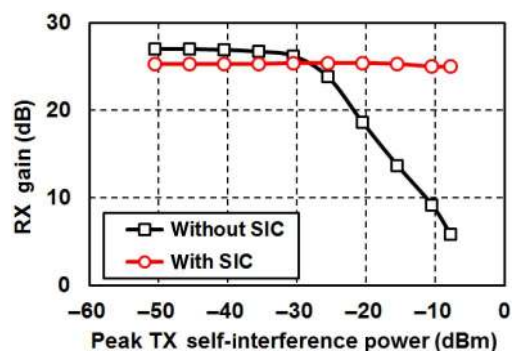
Fig. 22. Measured RX gain compression of a weak desired signal with and without SIC versus varying FD SI power level at the RX input.

compression of a desired signal (as opposed to nearly 22 dB of compression in the absence of SIC). SIC also improves the impact of RX nonlinearity on the SI itself, improving effective IB IIP3 from −20 to +2 dBm [Fig. 23(a)] and effective IB IIP2 from +10 to +68 dBm [Fig. 23(b)].

In the effective IB IIP3 measurement under SIC, there is no way to separate the canceller and RX IM3 contributions. We may infer their relative contributions from the fact that RX effective IB IIP3 should improve by the amount of SIC achieved (around 25 dB). The fact that it improves by 22 dB

Fig. 23. FD linearity measurement: RX IB IIP3 and IIP2 measurements with and without SIC for a two-tone IB SI of varying power. To be fair, we ensure that the two-tone TX signal u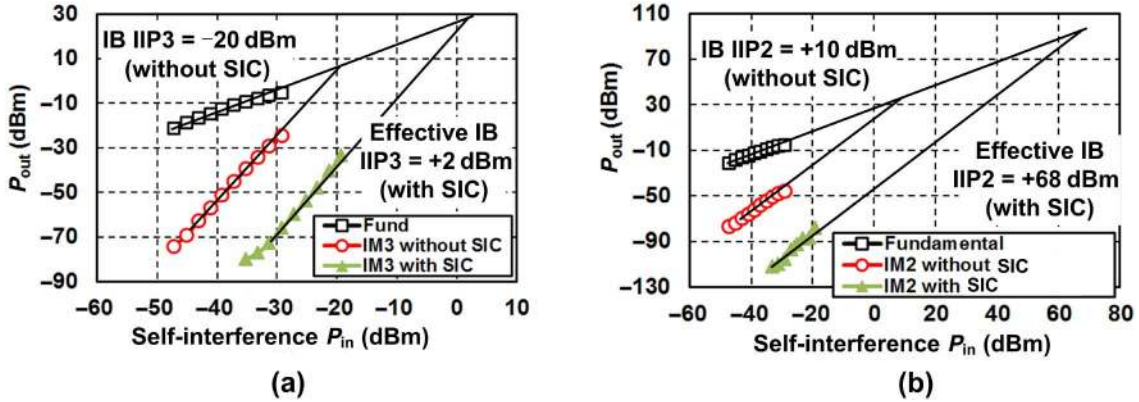ndergoes a cancellation of not more than 25 dB for these measurements [the average cancellation over the 25 MHz 20 dB SIC BW in Fig. 20(b)].
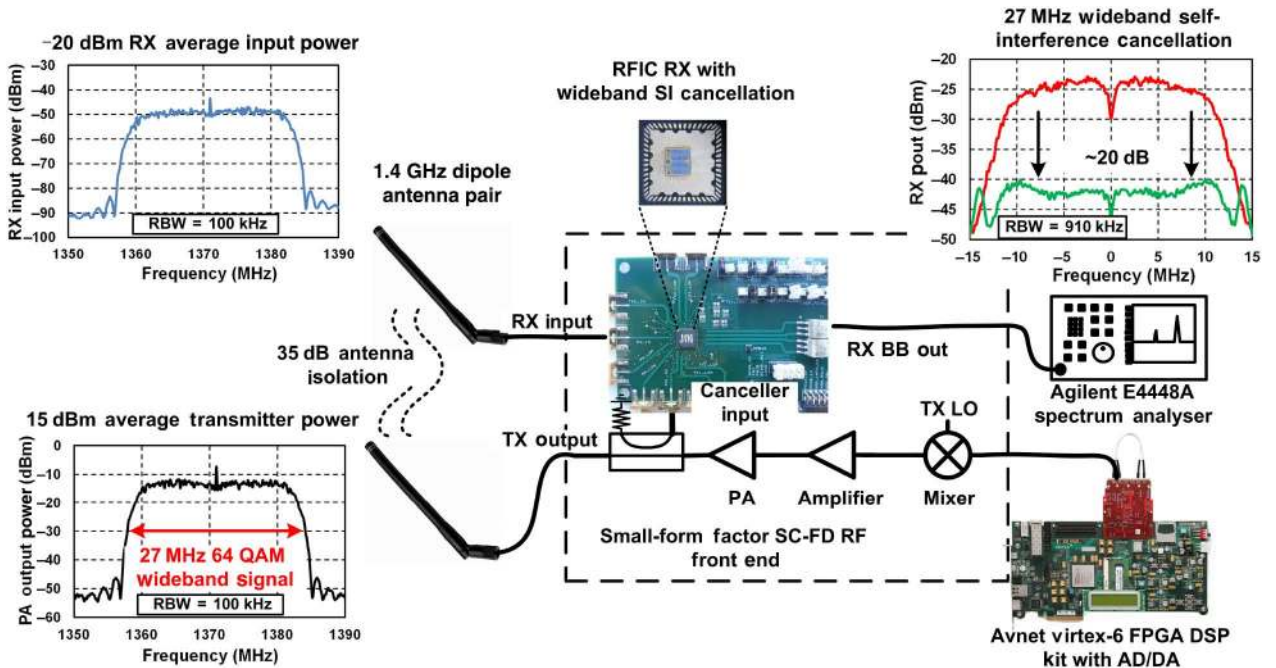


Fig. 24. Wireless demonstration of same-channel FD RF SIC of a 1.37 GHz 27 MHz-BW RRC-filtered 64-QAM signal across the 1.4 GHz antenna pair showing signal spectrum at various points and 20 dB SIC across the entire 27 MHz signal BW at the RX output. Off-the-shelf components are used to form the TX path.

indicates that the RX and canceller have roughly equal IM3 contribution, which is consistent with the system-level design guideline outlined in Section II-A. Even with both IM3 contributions, the effective IB IIP3 under SIC of $+2$ dBm exceeds the $+0.5$ dBm specification dictated by RX IM3 alone in Section II-A. Also, while IIP3 is an extrapolated metric, consistent IM3 levels are maintained up to a single-tone SI power level of $-19$ dBm, which corresponds to an average two-tone TX power of $+14$ dBm assuming 30 dB ISO. At that level, under SIC, the IM3 tones are 40 dB below the incident SI, exceeding the 37 dB requirement.

While IM2 was not considered in Section II, the required RX effective IIP2 under SIC is $P_{\text{TX,main}} - \text{ISO} - 3 + \text{SIC}_{\text{RF}} + \text{SIC}_{\text{BB}} = +19$ dBm, so that RX SI IM2 distortion does not exceed the residual SI after RF and analog SIC. The achieved RX effective IIP2 greatly exceeds this.

Fig. 24 illustrates a wireless same-channel FD SIC demonstration. A 27 MHz BW 64 QAM signal is transmitted using an off-the-shelf mixer and PA through one of the 1.4 GHz antennas. The modulated SI appears at the RX input with 35 dB antenna isolation. Using the proposed canceller, 20 dB cancellation across the entire 27 MHz SI BW is measured.

### D. Performance Summary and Comparison

Table I summarizes the system-level analysis and specifications presented in Section II and compares them to the measurement results just described. Table II compares the measurement results with prior art. This work achieves superior SIC BW, while achieving comparable SI power handling, NF degradation, and linearity enhancement under FDD SIC to [4] and supporting same-channel FD wireless. When

TABLE II
PERFORMANCE COMPARISON WITH THE STATE OF THE ART

| | RFIC 2014 [5] | JSSC 2006 [3] | JSSC 2014 [16] | RFIC 2014 [9] | ISSCC 2015 [11] | This work | | |
|---|---|---|---|---|---|---|---|---|
| | | | | | | RX with wideband SIC based on RF frequency-domain equalization | | |
| Architecture | LNA with passive transformer based TX leakage cancellation | LNA with LMS adaptive TX leakage filter | Noise-cancelling, SI cancelling (NC-SIC) RX | Mixer-first TRX with active baseband duplexing | Mixer-first receiver + SI-cancelling VM-downmixer | Without canc. | With cancellation (LC-based duplexer for FDD) | With cancellation (antenna pair for FD) |
| RX frequency (GHz) | 2.1 | 0.8 | 0.3–1.7 | 0.1–1.5 | 0.15–3.5 | 0.8–1.4 | | |
| RX noise figure (dB) | 2–2.5 (LNA only) | 1.4 (LNA only) | 4.2–5.6 | 5.2–7.7 | 6.3 | 4.8 | | |
| Gain (dB) | 19.8 (LNA only) | 16.5 (LNA only) | 19–34 | 53 | 24 (max.) | 27–42 | | |
| 20 dB cancellation BW (MHz) | N/R (frequency-flat RF SI canceller) | 1.23[a] (frequency-flat RF SI canceller) | 3[b]/3[c] (frequency-flat RF SI canceller) | N/R | N/R (frequency-flat RF SI canceller) | N/A | 17 (one filter)  24 (two filters) | 15 (one filter)  25 (two filters) |
| OOB IIP3 (dBm) | +3 (LNA only) | N/R | +12 | +22.5 | +22.0 | +17 | | |
| Effective OOB IIP3 with respect to SI (dBm) | N/R | N/R | +33[d] | N/A | N/A | N/A | +25 to 27[d] | N/A |
| OOB IIP2 (dBm) | N/R | N/R | N/R | N/R | N/R | +61 | | |
| Effective OOB IIP2 with respect to SI (dBm) | N/R | N/R | N/R | N/A | N/A | N/A | +90 | N/A |
| IB SC-FD P1 dB[e] (dBm) | N/A | N/A | N/A | −52.3/−17.3[f] | >+1.5[h] | −30.5 | N/A | »−8[f] |
| IB IIP3 (dBm) | N/A (LNA only) | N/A (LNA only) | N/R | −32.7 | +8/+16.2[i] | −20 | | |
| Effective IB IIP3 with respect to SI (dBm) | N/A (LNA only) | N/A (LNA only) | N/A | N/R | +19 | N/A | N/A | +2 |
| IB IIP2 (dBm) | N/A (LNA only) | N/A (LNA only) | N/R | N/R | N/R | +10 | | |
| Effective IB IIP2 with respect to SI (dBm) | N/A (LNA only) | N/A (LNA only) | N/A | N/R | N/R | N/A | N/A | +68 |
| Maximum handled peak SI power (dBm) | −25 | −28 | +2 | −17.3[g] | −18[j]/−10[k]/ +1.5[l] | N/A | −4 | −16[m]/−8[n] |
| NF degradation due to SI cancellation (dB) | 1–1.5 | 1.3 | 0.8 | N/R | 4–6 | N/A | 0.5 (one filter)  0.6 (two filters) | 0.9–1.1 (one filter)  1.1–1.3 (two filters) |
| RX power consumption (mW) | 10 (LNA only) | N/R | 75–83 | 43–56 | 23–56 | 63–69 | | |
| Canceller power consumption (mW) | 0 | 43 | 13–72 | | | N/A | 0–47 (Gm cells for one filter)  44 (LO at 1.35 GHz for one filter) | |
| SC-FD? | No | No | No | Yes | Yes | Yes | | |
| Antenna interface | Duplexer with single antenna | Duplexer with single antenna | Antenna pair/duplexer with single antenna | Single antenna | Antenna pair | Duplexer with single antenna (FDD)/ antenna pair (FD) | | |
| Technology (nm) | 40 CMOS | 250 CMOS | 65 CMOS | 65 CMOS | 65 CMOS | 65 CMOS | | |
| Active area (mm²) | 2.1 | N/A | 1.2 | 1.5 | 2 | 4.8 | | |

[a]10.8 dB average cancellation over 1.23 MHz across a CDMA SAW duplexer. [b]Across the 0.8/0.9 GHz LTE-like LC-based duplexer.
[c]Across the 1.4 GHz FD antenna pair. [d]Effective IIP3 under FDD SI cancellation from triple beat measurements.
[e]Power level of the FD IB TX SI that compresses a desired signal by 1 dB.
[f]Under FD SI cancellation. N/A: Not Applicable N/R: Not Reported.
[g]This is also the TX power limit due to the baseband duplexing scheme.
[h]1.3 dB RX compression. [i]Negative conductance OFF/ON. [j]SI power at which peak 69 dB SINDR is achieved.
[k]SI power level that allows a full-duplex link with +10 dBm TX power (20 dB antenna isolation) and −70 dBm distortion-limited noise floor.
[l]SI powe@1.3 dB RX compression.
[m]SI power level at which the RX meets the FD link budget proposed in Section II and Table I.
[n]Peak SI power level for which SIC is demonstrated.

compared with [11], a recently reported FD RFIC, this work achieves lower NF degradation and incorporates equalization functionality for wideband SIC. However, Ref. [11] achieves superior IB linearity with and without SIC due to a passive-mixer-first architecture. When compared with [9], another recently reported FD RFIC, this work exhibits superior SI power handling and IB linearity to SI.

Canceller DC power depends on antenna interface selectivity and desired SIC BW, and must be compared with the TX power consumption, as it can be powered down when the TX is inactive, or in the absence of a CW jammer for FDD. Measured canceller LO (TX LO) feedthrough to the RX input is about $-55$ dBm, low enough to not affect FDD/FD operation. Calibration techniques can further suppress the LO leakage [30].

## VI. CONCLUSION

Multiband FDD and FD wireless systems require TX SIC. We present a system-level analysis of FD transceivers that partitions the required SIC across RF, analog and digital domains, and derives the required performance specifications on the individual circuits comprising the RX and the RF canceller. The focus of this paper is on an approach to achieve wideband (e.g., $>20$ MHz) SIC in the RF domain. An approach based on FDE is proposed where reconfigurable BPFs are introduced in the canceller. The reconfigurable BPFs enable replication of not only the magnitude and phase of the frequency-selective antenna interface isolation but also their slopes in different sub-bands, thus greatly enhancing SIC BW. Furthermore, a two-port $G_m$-$C$ $N$-path filter with embedded variable attenuation and phase shift is introduced to implement the reconfigurable canceller BPFs. A proof-of-concept 0.8–1.4 GHz SIC RX prototype in 65 nm CMOS validates the claims and achieves $>20$ MHz cancellation BW (nearly $10\times$ improvement over conventional frequency-flat amplitude- and phase-based RF cancellers) across a custom-designed LTE-like 0.780/0.895 GHz duplexer for FDD and a 1.4 GHz antenna pair for FD wireless.

Several topics remain for future investigation, including tunable duplexers for FDD that can benefit from the proposed SIC technique, automatic and optimal canceller calibration algorithms and techniques, and the mitigation of the impact of LO phase noise.

## ACKNOWLEDGMENT

## APPENDIX

Here, the BPF parameters in (9) are derived from the antenna interface response $H_{\mathrm{SI}}(j\omega)$.

From (8), we have the $i$th BPF magnitude, phase, magnitude slope, and phase slope (group delay) as

$$|\hat{H}_i(j\omega)| = \frac{A_i}{\sqrt{1 + K(\omega)^2}},$$

$$\angle\hat{H}_i(j\omega) = \arctan K(\omega) - \phi_i,$$

$$\frac{d|\hat{H}_i(j\omega)|}{d\omega} = \frac{K(\omega)}{1 + K(\omega)^2}\frac{Q_i\omega_i}{\omega^2}(1 + \frac{\omega^2}{\omega_i^2})|\hat{H}_i(j\omega)|,$$

$$\frac{d\angle\hat{H}_i(j\omega)}{d\omega} = -\frac{1}{1 + K(\omega)^2}\frac{Q_i\omega_i}{\omega^2}(1 + \frac{\omega^2}{\omega_i^2}) \quad (12)$$

where $K(\omega) = Q_i\frac{\omega_i}{\omega}(1 - \frac{\omega^2}{\omega_i^2})$. Using $i$th BPF to emulate the antenna interface isolation magnitude, phase, magnitude slope, and phase slope (group delay) at the $i$th BPF cancellation frequency $\omega_{\mathrm{SIC},i}$ results in

$$|\hat{H}_i(j\omega_{\mathrm{SIC},i})| = |H_{\mathrm{SI}}(j\omega_{\mathrm{SIC},i})|,$$

$$\angle\hat{H}_i(j\omega_{\mathrm{SIC},i}) = \angle H_{\mathrm{SI}}(j\omega_{\mathrm{SIC},i}) + \pi,$$

$$\frac{d|\hat{H}_i(j\omega)|}{d\omega}\Big|_{\omega=\omega_{\mathrm{SIC},i}} = \frac{d|H_{\mathrm{SI}}(j\omega)|}{d\omega}\Big|_{\omega=\omega_{\mathrm{SIC},i}},$$

$$\frac{d\angle\hat{H}_i(j\omega)}{d\omega}\Big|_{\omega=\omega_{\mathrm{SIC},i}} = \frac{d\angle H_{\mathrm{SI}}(j\omega)}{d\omega}\Big|_{\omega=\omega_{\mathrm{SIC},i}}. \quad (13)$$

Finally, the BPF parameters in (9) can be solved from (12) and (13) as [repeat (9) with shorthand notation values given]

$$\phi_i = \angle H_{\mathrm{SI}}(j\omega_{\mathrm{SIC},i}) + \arctan\frac{B}{|H_{\mathrm{SI}}(j\omega_{\mathrm{SIC},i})|} + \pi,$$

$$\omega_i = \sqrt{\frac{1+P}{1-P}}\omega_{\mathrm{SIC},i},$$

$$Q_i = -\frac{B}{|H_{\mathrm{SI}}(j\omega_{\mathrm{SIC},i})|}\frac{1+P}{2P},$$

$$A_i = \sqrt{1 + K(\omega_{\mathrm{SIC},i})^2}|H_{\mathrm{SI}}(j\omega_{\mathrm{SIC},i})| \quad (14)$$

where $\omega_{\mathrm{SIC},i}$ is the cancellation frequency for the $i$th BPF, $B = \frac{\frac{d|H_{\mathrm{SI}}(j\omega)|}{d\omega}\big|_{\omega=\omega_{\mathrm{SIC},i}}}{\frac{d\angle H_{\mathrm{SI}}(j\omega)}{d\omega}\big|_{\omega=\omega_{\mathrm{SIC},i}}}$, $K(\omega_{\mathrm{SIC},i}) = -B/|H_{\mathrm{SI}}(j\omega_{\mathrm{SIC},i})|$, $P = \frac{B^2|H_{\mathrm{SI}}(j\omega_{\mathrm{SIC},i})|}{(B^2+|H_{\mathrm{SI}}(j\omega_{\mathrm{SIC},i})|^2)}(\frac{d|H_{\mathrm{SI}}(j\omega)|}{d\omega}\big|_{\omega=\omega_{\mathrm{SIC},i}}\omega_{\mathrm{SIC},i})^{-1}$.

## REFERENCES

[1] A. Roessler and M. Kottkamp, "LTE-advanced (3GPP Rel.11) technology introduction," Rohde and Schwarz, Munich, Germany, White Paper, Jul. 2013.

[2] A. Goel, B. Analui, and H. Hashemi, "Tunable duplexer with passive feed-forward cancellation to improve the RX-TX isolation," *IEEE Trans. Circuits Syst. I. Reg. Papers*, vol. 62, no. 2, pp. 536–544, Feb. 2015.

[3] V. Aparin, G. Ballantyne, C. Persico, and A. Cicalini, "An integrated LMS adaptive filter of TX leakage for CDMA receiver front ends," *IEEE J. Solid-State Circuits*, vol. 41, no. 5, pp. 1171–1182, May 2006.

[4] J. Zhou, P. Kinget, and H. Krishnaswamy, "A blocker-resilient wideband receiver with low-noise active two-point cancellation of $>0$ dBm TX leakage and TX noise in RX band for FDD/co-existence," in *IEEE Int. Solid-State Circuits Conf. (ISSCC) Dig. Tech. Papers*, Feb. 2014, pp. 352–353.

[5] T. Zhang, A. R. Suvarna, V. Bhagavatula, and J. C. Rudell, "An integrated CMOS passive transmitter leakage suppression technique for FDD radios," in *Proc. IEEE Radio Freq. Integr. Circuits Symp. (RFIC'14)*, 2014, pp. 43–46.

[6] A. Sabharwal, P. Schniter, D. Guo, D. Bliss, S. Rangarajan, and R. Wichman, "In-band full-duplex wireless: Challenges and opportunities," *IEEE J. Sel. Areas Commun.*, vol. 32, no. 9, pp. 1637–1652, Sep. 2014.

[7] D. Bharadia, E. McMilin, and S. Katti, "Full duplex radios," in *Proc. ACM SIGCOMM Conf.*, 2013, pp. 375–386.

[8] B. Debaillie *et al.*, "Analog/RF solutions enabling compact full-duplex radios," *IEEE J. Sel. Areas Commun.*, vol. 32, no. 9, pp. 1662–1673, Sep. 2014.

[9] D. Yang and A. Molnar, "A widely tunable active duplexing transceiver with same-channel concurrent RX/TX and 30 dB RX/TX isolation," in *Proc. IEEE Radio Freq. Integr. Circuits Symp.*, Jun. 2014, pp. 321–324.

[10] J. Zhou, T.-H. Chuang, T. Dinc, and H. Krishnaswamy, "A receiver with reconfigurable self-interference cancellation based on RF frequency-domain equalization supporting >20 MHz cancellation bandwidth for FDD, co-existence and same-channel full duplex applications," in *IEEE Int. Solid-State Circuits Conf. (ISSCC) Dig. Tech. Papers*, Feb. 2015, pp. 342–343.

[11] D.-J. van den Broek, E. Klumperink, and B. Nauta, "A self-interference-cancelling receiver for in-band full-duplex wireless with low distortion under cancellation of strong TX leakage," in *IEEE Int. Solid-State Circuits Conf. (ISSCC) Dig. Tech. Papers*, Feb. 2015, pp. 1–3.

[12] M. Duarte, C. Dick, and A. Sabharwal, "Experiment-driven characterization of full-duplex wireless systems," *IEEE Trans. Wireless Commun.*, vol. 11, no. 12, pp. 4296–4307, Dec. 2012.

[13] T. Dinc, A. Chakrabarti, and H. Krishnaswamy, "A 60 GHz same-channel full-duplex CMOS transceiver and link based on reconfigurable polarization-based antenna cancellation," in *Proc. IEEE Radio Freq. Integr. Circuits Symp. (RFIC'15)*, 2015, pp. 31–34.

[14] T. Dinc and H. Krishnaswamy, "A T/R antenna pair with polarization-based wideband reconfigurable self-interference cancellation for simultaneous transmit and receive," in *Proc. IEEE MTT-S Int. Microw. Symp. (IMS'15)*, 2015, pp. 1–4.

[15] J. Marasevic, J. Zhou, H. Krishnaswamy, Y. Zhong, and G. Zussman, "Resource allocation and rate gains in practical full-duplex systems," in *Proc. ACM SIGMETRICS*, Jun. 2015, pp. 1–16.

[16] J. Zhou, A. Chakrabarti, P. Kinget, and H. Krishnaswamy, "Low-noise active cancellation of transmitter leakage and transmitter noise in broadband wireless receivers for FDD/co-existence," *IEEE J. Solid-State Circuits*, vol. 49, no. 12, pp. 3046–3062, Dec. 2014.

[17] H. Hashemi, T.-S. Chu, and J. Roderick, "Integrated true-time-delay-based ultra-wideband array processing," *IEEE Commun. Mag.*, vol. 46, no. 9, pp. 162–172, Sep. 2008.

[18] L. Franks and I. Sandberg, "An alternative approach to the realization of network transfer functions: The N-path filter," *Bell Syst. Tech. J.*, vol. 39, no. 5, pp. 1321–1350, Sep. 1960.

[19] A. Mirzaei, H. Darabi, A. Yazdi, Z. Zhou, E. Chang, and P. Suri, "A 65 nm CMOS quad-band SAW-less receiver SOC for GSM/GPRS/EDGE," *IEEE J. Solid-State Circuits*, vol. 46, no. 4, pp. 950–964, Apr. 2011.

[20] A. Ghaffari, E. Klumperink, M. C. M. Soer, and B. Nauta, "Tunable high-Q N-path band-pass filters: Modeling and verification," *IEEE J. Solid-State Circuits*, vol. 46, no. 5, pp. 998–1010, May 2011.

[21] M. Darvishi, R. van der Zee, E. Klumperink, and B. Nauta, "Widely tunable 4th order switched $G_m$-$C$ band-pass filter based on N-path filters," *IEEE J. Solid-State Circuits*, vol. 47, no. 12, pp. 3105–3119, Dec. 2012.

[22] H. Khatri, P. Gudem, and L. Larson, "An active transmitter leakage suppression technique for CMOS SAW-less CDMA receivers," *IEEE J. Solid-State Circuits*, vol. 45, no. 8, pp. 1590–1601, Aug. 2010.

[23] A. Sahai, G. Patel, C. Dick, and A. Sabharwal, "On the impact of phase noise on active cancellation in wireless full-duplex," *IEEE Trans. Veh. Technol.*, vol. 62, no. 9, pp. 4494–4510, Nov. 2013.

[24] M. Soer, E. Klumperink, P.-T. de Boer, F. van Vliet, and B. Nauta, "Unified frequency-domain analysis of switched-series-RC passive mixers and samplers," *IEEE Trans. Circuits Syst. I, Reg. Papers*, vol. 57, no. 10, pp. 2618–2631, Oct. 2010.

[25] N. Reiskarimian, J. Zhou, T.-H. Chuang, and H. Krishnaswamy, "Analysis and design of two-port N-path band-pass filters with embedded phase shifting," *IEEE Trans. Circuits Syst. II, Exp. Briefs*, 2015, to be published.

[26] D. Murphy *et al.*, "A blocker-tolerant, noise-cancelling receiver suitable for wideband wireless applications," *IEEE J. Solid-State Circuits*, vol. 47, no. 12, pp. 2943–2963, Dec. 2012.

[27] H. Khatri, P. Gudem, and L. Larson, "Distortion in current commutating passive CMOS downconversion mixers," *IEEE Trans. Microw. Theory Techn.*, vol. 57, no. 11, pp. 2671–2681, Nov. 2009.

[28] M. Omer, R. Rimini, P. Heidmann, and J. S. Kenney, "A PA-noise cancellation technique for next generation highly integrated RF front-ends," in *Proc. IEEE Radio Freq. Integr. Circuits Symp. (RFIC'12)*, 2012, pp. 471–474.

[29] "ACMD-7612 miniature UMTS band I duplexer data sheet," Avago Technologies, San Jose, CA, USA, Sep. 2007.

[30] S. Jayasuriya, D. Yang, and A. Molnar, "A baseband technique for automated LO leakage suppression achieving < −80 dBm in wideband passive mixer-first receivers," in *Proc. IEEE Custom Integr. Circuits Conf. (CICC)*, Sep. 2014, pp. 1–4.

**Jin Zhou** (S'11) received the B.S. degree in electronics science and technology from Wuhan University, Wuhan, China, in 2008, and the M.S. degree in microelectronics from Fudan University, Shanghai, China, in 2011. He is currently working toward the Ph.D. degree in electrical engineering at Columbia University, New York, NY, USA.

From 2008 to 2011, he was a Research Assistant with Fudan University and worked on frequency synthesizer for multistandard wireless transceiver. From 2011 to 2012, he was with MediaTek Singapore, Singapore, and worked on PLL/DLL for cellular and wireless applications.

Mr. Zhou was the recipient of the 2010 IEEE International Conference on Solid-State and Integrated Circuit Technology (ICSICT) Excellent Student Paper Award, and the 2015–2016 Qualcomm Innovation Fellowship.

**Tsung-Hao (Jeffrey) Chuang** (S'13) received the B.S. degree in electrical engineering from National Taiwan University, Taipei, Taiwan, in 2010, and the M.S. degree in electrical engineering from Columbia University, New York, NY, USA, in 2013. He is currently working toward the Ph.D. degree in electrical engineering at Columbia University, New York, NY, USA.

Since 2011, he has been a Research Assistant with the Department of Electrical Engineering, Columbia University, and has worked on the design of fast-hopping phase-locked loops, radio-frequency LO generation circuitry, and millimeter-wave power amplifiers. From 2013 to 2014, he held internship positions at Bell Laboratories, Alcatel-Lucent, Inc., Murray Hill, NJ, USA, and Epoch Microelectronics, Inc., Valhalla, NY, USA, and worked on millimeter-wave building blocks for wireline transceiver and vehicular radar system, respectively.

**Tolga Dinc** (S'09) received the B.S. and M.S. degrees in electrical engineering from Sabanci University, Istanbul, Turkey, in 2010 and 2012, respectively. He is currently working toward the Ph.D. degree in electrical engineering at Columbia University, New York, NY, USA.

His research interests include end-to-end design of millimeter-wave integrated systems for high-speed communication applications.

Mr. Dinc was the recipient of a 2010 MTT-S Undergraduate/Pre-Graduate Scholarship Award and a 2012 Sabanci University Gursel Sonmez Research Award. He was also the recipient of the IEEE RFIC Symposium Best Student Paper Award—First Place in 2015.

**Harish Krishnaswamy** (S'03–M'09) received the B.Tech. degree from the Indian Institute of Technology, Madras, India, in 2001, and the M.S. and Ph.D. degrees from the University of Southern California (USC), Los Angeles, CA, USA, in 2003 and 2009, respectively, all in electrical engineering.

In 2009, he joined the Department of Electrical Engineering, Columbia University, New York, NY, USA, where he is currently an Associate Professor. His research interests include integrated devices, circuits, and systems for a variety of RF, millimeter- and submillimeter-wave applications.

Dr. Krishnaswamy serves as a member of the Technical Program Committee (TPC) of several conferences, including the IEEE International Solid-State Circuits Conference (2015/2016–present) and the IEEE RFIC Symposium (2013–present). He was the recipient of the IEEE International Solid-State Circuits Conference (ISSCC) Lewis Winner Award for Outstanding Paper in 2007, the Best Thesis in Experimental Research Award from the USC Viterbi School of Engineering in 2009, the Defense Advanced Research Projects Agency (DARPA) Young Faculty Award in 2011, a 2014 IBM Faculty Award, and the 2015 IEEE RFIC Symposium Best Student Paper Award—First Place.